

Common Envelope Evolution on the Asymptotic Giant Branch: Towards Building a Simple Model

*A thesis Submitted
in Partial Fulfilment of the Requirements
for the Degree of
MASTER OF SCIENCE*

by
SOUMIK BHATTACHARYYA



to the
School of Physical Sciences
National Institute of Science Education and Research
Bhubaneswar
15th July, 2023

DECLARATION

I hereby declare that I am the sole author of this thesis in partial fulfillment of the requirements for a postgraduate degree from National Institute of Science Education and Research (NISER). I authorize NISER to lend this thesis to other institutions or individuals for the purpose of scholarly research.

Signature of the Student

Date:

The thesis work reported in the thesis entitled *Common Envelope Evolution on the Asymptotic Giant Branch: Towards Building a Simple Model* was carried out under my supervision, in the school of physical sciences at NISER, Bhubaneswar, India.

Signature of the thesis supervisor

School: School of Physical Sciences, NISER

Date:

ACKNOWLEDGEMENTS

As I reflect on my journey of five years, I am thankful to the many individuals who have made this experience wonderful and enjoyable. First and foremost, I would like to express my sincere gratitude to my project supervisor, Dr. Luke Chamandy, for his invaluable guidance and encouragement throughout the project. His expertise, insightful discussions, and valuable suggestions have played a crucial role in shaping the direction and quality of the work. I consider myself fortunate to have had the opportunity to work with him, and I am truly grateful for his mentorship and support.

I would also like to extend my appreciation to Dr. Adam Frank, Dr. Eric Blackman, and their lab group at the Department of Physics and Astronomy, the University of Rochester, for their support and for providing me with access to the simulation data and resources.

I am grateful to Dr. Baowei Liu and the Center for Integrated Research Computing (CIRC) at the University of Rochester for generously providing me with the extensive computational resources necessary to carry out this research. Their support has been instrumental in handling the computational challenges involved in the project.

I am deeply thankful to my previous guide, Dr. Guneshwar Thangjam, from the School of Earth and Planetary Sciences, whose mentorship and guidance sparked my interest and passion for research. His insights and encouragement have left an indelible impact on my academic journey.

I would also like to acknowledge the School of Physical Sciences for offering me the opportunity to pursue a project aligned with my research interests. Their support has fostered an environment conducive to growth and exploration.

In addition, I express my heartfelt appreciation to my friends, including Jyoth-

ish, Nikhil, Nishant, Ravi, Priyanka, Nelson, Suraj, Arnab, Dwaipayan, Priyobrata, Fida, Rion, Aniruddha, Tamoghna, Hiranmay, Ananya, Archisman, and many others. Their companionship, camaraderie, and unwavering support have provided me with strength, motivation, and cherished memories throughout this journey.

Finally, I am deeply grateful to my family and loved ones for their unwavering support and encouragement. I would like to express my heartfelt gratitude to my parents, who have been a constant source of belief and support throughout my journey. During the most challenging moments, I find solace in knowing that I have their unconditional belief in me. Their love and encouragement have been invaluable in shaping my path and giving me the strength to overcome obstacles.

To all those who have contributed to my growth, both personally and academically, I offer my deepest appreciation and gratitude. This journey would not have been the same without your presence and support.

ABSTRACT

Common Envelope (CE) is a significant yet poorly understood process in the evolution of binary star systems. Observing CE directly is practically impossible due to its short duration, and simulating it computationally poses challenges due to computational demands and the diverse nature of binary systems undergoing CE. This research focuses on analyzing a simulated binary system, with an Asymptotic Giant Branch (AGB) star as the primary core and a companion star of equal mass. The simulation extends for approximately 40 orbital revolutions, although a stationary orbit is not achieved. The study investigates the drag force exerted by gas particles on the secondary mass and compares it to previous simulation-based works. Additionally, the torque applied to both stars by the gas medium is calculated and analyzed. Furthermore, the research evaluates the torque exerted by a certain percentage of gas and determines the amount of gas required to achieve a comparable torque to the total torque. The study then aims to model the torque exerted on the stars by treating the bulk of gas inside the equidensity surface as a homogeneous and prolate ellipsoidal body. By parameterizing the ellipsoid and obtaining the semi-axes (A , B , C) and the lag angle between the binary system axis and the major axis of the ellipsoid ($\Delta\phi$), the torque applied to both stars within the bulk of gas is calculated from the potential energy inside the fitted ellipsoid. The calculated torque is found to be consistent with the torque calculated from the drag force. Moreover, an expression for the binary separation is developed and successfully modeled within the timescale of evolution.

Contents

1	Introduction	1
2	Theory	6
2.1	Potential at an interior point of a homogeneous ellipsoid	6
2.1.1	Oblate and Prolate Spheroid	7
2.2	Calculating the torque from potential	8
2.3	Binary Separation	10
3	Methods	11
3.1	AstroBEAR	11
3.2	Simulation parameters	11
3.3	VisIt as an analysing tool	13
3.4	Evolution of the system	13
4	Results and Discussion	17
4.1	Orbital Separation	17
4.2	Drag Force Evolution	19
4.3	Evolution of Torque	22
4.4	Selection of Ellipsoidal Surface	23
4.5	Fitting the Ellipsoids	25
4.6	Parameter Evolution	26
4.7	The Time-Dependant Model of Torque	30
4.7.1	Taking the approximation of a prolate ellipsoid case	30
4.7.2	Modelling the torque	31
4.8	Modelling the binary separation	33
5	Summary and Conclusions	34
	Appendix A Potential of Homoeoids and Ellipsoids	37

List of Figures

1.1	Schematic of canonical common envelope evolution. [Courtesy. Ivanova et al. [2020]]	2
3.1	Gas density, ρ , in $g.cm^{-3}$ on orbital plane in the initial frame of the simulation in log-pseudocolor plot. The numbers 0 and 1 represent primary core and secondary, respectively.	12
3.2	Pseudocolor-contour plot for gas density through orbital plane at $t [d] = 0.0, 23.1, 46.3, 69.4, 92.6$ and 115.7	14
3.3	Pseudocolor-contour plot for gas density through orbital plane at $t [d] = 138.9, 162.3, 185.2, 208.3, 231.5$ and 254.6	15
4.1	Separation between two particle cores in orbital plane as a function of time	17
4.2	Motion of the center of mass of the particle cores in orbital plane	18
4.3	Orbit of particle cores in orbital plane	18
4.4	Top: (i) The ϕ component of drag force in lab frame is plotted in dark-grey dashed line; (ii) The force along velocity component is plotted in gold dashed line; (iii) The azimuthal component of the drag force on particle 2 in rest frame of particle 1 is plotted in black solid line; (iv) The orbital separation is plotted on the right axis as a reference. Bottom: Results from Chamandy et al. [2020], which calculates the azimuthal component of drag force in rest frame of particle 1 for an AGB and a RGB primary core star (Courtesy: Chamandy et al. [2020])	20
4.5	The z-component of torque calculated from force and orbital angular momentum has been plotted in solid black line and yellow dashed line, respectively. Orbital separation has been plotted on the right y-axis.	22
4.6	Ratio of torque exerted on the binary system by some amount of gas and all of gas is plotted for different frames from the simulation is shown.	24
4.7	The left y-axis of the plot shows the torque as a function of time. The torque applied by all of the gas is represented by the black dashed line, while the torque applied by a certain percentage of gas is shown in blue. On the right y-axis, we display the ratio of both the torques.	24
4.8	The contours of ellipses and fitted ellipses for orbital plane (left) and perpendicular plane (right) are shown for two different time-frames.	26
4.9	Evolution of semi-major axis (A) with time.	27
4.10	Evolution of semi-minor axis in orbital plane (B) with time.	27
4.11	Evolution of semi-minor axis in perpendicular plane (C) with time.	28
4.12	Evolution of lag between binary axis and major axis of the ellipsoid ($\Delta\phi$) with time.	28
4.13	Evolution of the ratio A/a with time.	29
4.14	Evolution of the ratio B/A with time.	29
4.15	Evolution of the ratio C/A with time.	30
4.16	Time evolution of the ratio C/B	31

LIST OF FIGURES

4.17 The torque has been calculated in two different methods. The solid black line shows the torque calculated from this homogeneous ellipsoid model (equation 2.10) and the dashed gold line shows the torque calculated from drag force.	31
4.18 The torque has been calculated from the homogeneous ellipsoid model with the approximation $C/A = 0.664$	32
4.19 The torque has been calculated from the homogeneous ellipsoid model with the approximations $C/A = 0.664$ and $\Delta\phi = 25 \text{ rad}$	33
4.20 The black dashed line and red solid line are respectively the actual separation from simulation and the separation from model.	33

List of Tables

3.1 Parameters of the simulation analysed in this work	11
--	----

Chapter 1

Introduction

In 1976, [Bohdan Paczynski](#) referred to a particular "cataclysmic binary" with an orbital period of just about 12 hours, V471 Tau, and wondered if theories of stellar evolution during that time could explain the small separation and short period of the system. V471 Tau is located at the open star cluster Hyades and consists of a white dwarf and a main sequence star. The age of the cluster was known at that time, as was the approximate mass ($2M_{\odot}$) of the stars in the cluster which were leaving the main sequence. Paczynski noted that the observed white dwarf star had to overcome a asymptotic giant branch phase with an approximate radius of $600R_{\odot}$ and orbital period in the order of years at least. He cited [Webbink \[1975\]](#) and his personal discussions with [Ostriker](#) and argued that the stars must have gone through an intermediate phase of rapid mass exchange in order to reach the currently observed state. The most natural way to explain this mass exchange is a "Common Envelope Evolution (CEE)".

CEE is a short-lived, yet vital process in the evolution of a large number and wide-variety of binary systems. As the name suggests, a common envelope phase is defined as the evolutionary phase when both the stars, revolving around their centre of mass, is immersed in a single, shared envelope [[Bohdan Paczynski, 1976](#), [Ivanova et al., 2013](#)]. Usually, the term CE is used to describe a situation in which the envelope is not co-rotating with the binary and is not necessarily in hydrostatic equilibrium [[Iben and Livio, 1993](#)]. Examples of systems that have undergone this phase or are experiencing such a phase almost certainly includes bipolar planetary nebulae (pNe)

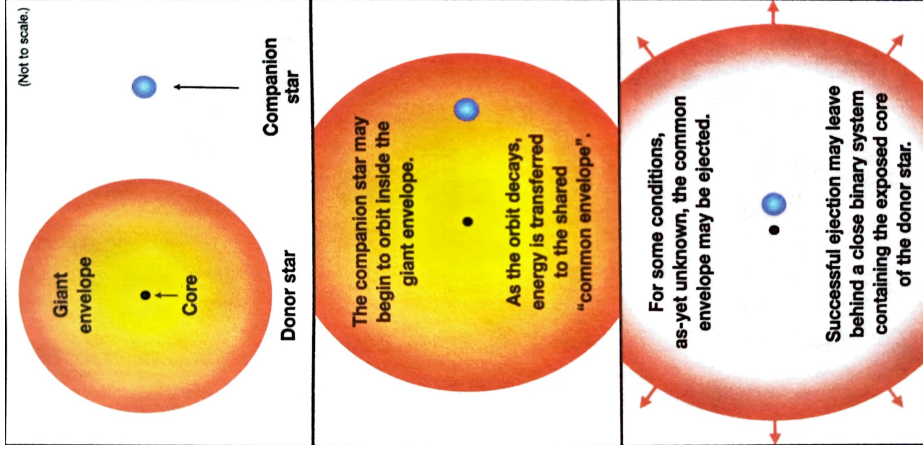


Figure 1.1: Schematic of canonical common envelope evolution. [Courtesy. [Ivanova et al. \[2020\]](#)]

[[Soker, 1994](#), [Reyes-Ruiz and López, 1999](#), [Soker and Rappaport, 2000, 2001](#), [Blackman et al., 2001](#), [Balick and Frank, 2002](#), [Nordhaus and Blackman, 2006](#), [Nordhaus et al., 2007](#), [Witt et al., 2009](#)]; SPRITE [[Kasliwal et al., 2017](#)], transient luminosity objects such as ILOT/ ILRT/ LRT [[Kashi and Soker, 2016](#), [Soker and Kashi, 2016](#), [Blagorodnova et al., 2017a,b](#), [Pastorello et al., 2019](#)]; progenitors of Type Ia supernovae [[Iben and Tutukov, 1984](#), [Han and Podsiadlowski, 2004](#), [Ruiter et al., 2011](#), [Meng and Podsiadlowski, 2017](#)]; progenitors of gravitational wave generating merger [[Kalogera et al., 2007](#), [Ivanova et al., 2013](#), [Belczynski et al., 2014](#)]; progenitors of double neutron stars [[Brown, 1995](#), [Dewi et al., 2006](#), [Ivanova, 2011](#)] etc.

Efforts are currently being made to gain observational knowledge on such transient events. The Legacy Survey of Space and Time (LSST) project of Vera C. Rubin Observatory [[Hambleton et al., 2022](#)], SPitzer InfraRed Intensive Transients Survey (SPIRITS) [[Kasliwal, 2016](#)] are some of the examples. However, it is needless to mention that studying CEE through observational methods is intensely challenging due to its short duration compared to astronomical timescale. For example, expected

lifetime of the CEE phase in a star’s life is in the order of decades or even shorter, making it an extremely rare event to observe. Additionally, the physical complexity and numerical demands of CEE make it difficult to unravel the underlying mechanisms either numerically or analytically. Early analytic formalism of CEE [Livio and Soker, 1988, De Kool, 1990, Iben and Livio, 1993] was performed with simplified models involving energy or angular momentum conservation of the system. The general goal was to model the evolutionary phases of a hypothetical binary system to reach a phase which complements currently observed highly evolved binaries. Some of the early simulation-based works include Rasio and Livio [1996], Sandquist et al. [1998], Sandquist et al. [2000], Lombardi Jr et al. [2006]. Over the course of last decade, an increasing number of codes including both smoothed particle hydrodynamics (SPH) and grid-based (often adaptive or moving mesh) models have been adapted to model CEE. A comparison study between previous simulations, performed by Iaconi et al. [2016] and Iaconi et al. [2018] have found that an increased resolution in the code can increase the unbound mass present in the system in later stages of evolution. The simulation that has been studied and analysed in this work utilized the 3-dimensional Adaptive Mesh Refinement (AMR) multiphysics code AstroBEAR [Cunningham et al., 2009, Carroll-Nellenback et al., 2013], which is discussed briefly in following chapters.

However, the extensive numerical demands are not the only issues with studying CEE through simulations. The possibility of a vast range of binary systems going into such a phase also makes it difficult to generalise it. In a general CE stage, it is expected that the companion would inspiral through the envelope and the envelope would gain energy and angular momentum from the process. Depending upon the energetic, the envelope could be ejected in later stages, leaving a stable and compact

system of binary stars, or the system may lead to a gravitational wave generating merger. Some of the other important parameters are the mass of the primary star, the mass ratio of the two stars, nature of the companion (main sequence star/ white dwarf/ neutron star etc.), the circumstellar environment etc.

In all types of these systems, however, accretion of gas particles plays a pivotal role to explain both envelope ejection and inspiral of the stars. Efforts have been made to incorporate Bondi-Hoyle-Lyttleton (BHL) [Hoyle and Lyttleton, 1939, 1940, Bondi and Hoyle, 1944, Bondi, 1952, Edgar, 2004] and Eddington-limited accretion model to explain the accretion rate in performed simulations [Ricker and Taam, 2007, 2012, MacLeod and Ramirez-Ruiz, 2014, 2015, MacLeod et al., 2017]. However, the rate in the dynamical system has been found to be exceeding the Eddington limit, but still significantly below the BHL accretion rate [Chamandy et al., 2018]. In any case, the dynamical drag force exerted on the secondary star by its accreted material is expected to play an important role in the inspiral of the system. The drag force on an accreting body in astronomical systems is caused by the gravitational focusing of material behind the accreting body [Chandrasekhar, 1943, Ostriker, 1999]. The drag force in common envelope evolution in a gaseous medium has been calculated and discussed in detail in Ostriker [1999].

As we compare results from previous simulations [MacLeod et al., 2017, Chamandy et al., 2019a], we find that the drag force calculated in late time of simulations is not in good agreement with theory. Reichardt et al. [2018], Ostriker [1999], Chamandy et al. [2019a] have explored possible improvements for theory at late times. The conventional theoretical formula for drag force [Ostriker, 1999] is dependant of the Mach number (\mathcal{M}_∞) and this could account for the small values observed for drag force at

late times. Also, the theoretical formula is also not well adjusted for late times as the orbital separation goes too small. Another possibility to explain the reduction in drag force is a reduced magnitude of relative velocity between particle (core of the star) and gas [Reichardt et al., 2018]. However, reasonable changes in initial gas density, velocity with respect to companion star and sound speed still could not explain the difference in calculated drag force and theoretical predictions [Chamandy et al., 2019a]. Another possibility that could help understand the discrepancy is to introduce a '*hydrodynamic drag*' in the particle-bulge system [Chamandy et al., 2019a].

At this point of discussion, considering the large variety of systems and the complexity of each system, we recognise the importance of building a simple analytic model for the common envelope. A simple equidensity ellipsoidal model for gas envelope of a binary system (Massive Black Hole in their case) was proposed by Escala et al. [2004]. Some of the features of their simplified model involves a constant lag ($\Delta\phi$) between binary axis and major axis of the ellipse on orbital plane and the ellipsoid being a homogeneous one. We take our motivation from their work and try to construct a similar model for common envelope evolution.

The expression for torque at an interior point of a homogeneous ellipsoid is formulated in chapter 2. The numerical methods, initial parameters and tools used for analyzing the simulation have been discussed in chapter 3. Chapter 4 contains observation and results from simulation including orbital evolution, evolution of the drag force and torque exerted on the body, morphology of the inner CE, choice of equidensity surface of the ellipsoid and results from our derived model of torque and binary separation. Chapter 5 summarizes the content of the thesis and concludes with a discussion on possible directions of future work.

Chapter 2

Theory

In order to model the torque as a function of time, we can model the equidensity ellipsoidal surface as a function of time and find out the torque applied by such a system. Although we have a heterogeneous ellipsoid producing the torque, we consider a homogeneous ellipsoid to keep our elementary model simple.

2.1 Potential at an interior point of a homogeneous ellipsoid

The analytical closed form expression for the gravitational potential of an ellipsoidal mass has been studied by [Lamb \[1879\]](#), [Kirchhoff \[1897\]](#) in great detail. The topic has further been discussed by [Chandrasekhar \[1969, Chapter 3\]](#). The detailed derivation is discussed in appendix [??](#). We can write down the final form for an ellipsoid with semi-axes A, B, C such that $A \geq B \geq C$,

$$\begin{aligned}\Phi_{int} &= -\pi G \rho (\chi_0 - (\alpha_0 x^2 + \beta_0 y^2 + \gamma_0 z^2)) \\ &= \pi G \rho (\alpha_0 x^2 + \beta_0 y^2 + \gamma_0 z^2 - \chi_0)\end{aligned}\tag{2.1}$$

where

$$\begin{aligned}
 \chi_0 &= ABC \int_0^\infty \frac{du}{\Delta} , \\
 \alpha_0 &= \frac{2BC}{A^2 \sin^3 \phi \sin^2 \theta} [F(\theta, \phi) - E(\theta, \phi)] , \\
 \beta_0 &= \frac{2BC}{A^2 \sin^3 \phi \sin^2 \theta \cos^2 \theta} \left[E(\theta, \phi) - F(\theta, \phi) \cos^2 \theta - \frac{C}{B} \sin^2 \theta \sin \phi \right] , \\
 \gamma_0 &= \frac{2BC}{A^2 \sin^3 \phi \cos^2 \theta} \left[\frac{B}{C} \sin \phi - E(\theta, \phi) \right] , \\
 u &= C^2 \tan^2 \theta , \\
 du &= 2C^2 \sin \theta \sec^3 \theta d\theta \text{ and} \\
 \Delta &= (C^2 \tan^2 \theta + C^2)^{1/2} (C^2 \tan^2 \theta + A^2)^{1/2} (C^2 \tan^2 \theta + B^2)^{1/2} \\
 &= (u + C^2)^{1/2} (u + A^2)^{1/2} (u + B^2)^{1/2}
 \end{aligned} \tag{2.2}$$

$F(\theta, \phi)$ and $E(\theta, \phi)$ are the standard incomplete elliptic integrals of first and second kind.

$$\begin{aligned}
 F(\theta, \phi) &= \int_0^\phi (1 - \sin^2 \theta \sin^2 \phi)^{-t} d\phi \\
 E(\theta, \phi) &= \int_0^\phi (1 - \sin^2 \theta \sin^2 \phi)^t d\phi
 \end{aligned} \tag{2.3}$$

θ and ϕ are defined by,

$$\begin{aligned}
 \sin \theta &= \left(\frac{A^2 - B^2}{A^2 - C^2} \right)^{\frac{1}{2}} \\
 \cos \phi &= \frac{C}{A}
 \end{aligned} \tag{2.4}$$

2.1.1 Oblate and Prolate Spheroid

The generalised form for the constants of the solution for the case $A > B > C$ are given in equation 3.1-3.4. These can further be reduced for the cases [Binney and Tremaine, 2011]:

1. **Oblate** ($A = B > C$):

$$\begin{aligned}\chi_0 &= 2 \frac{1 - e^2}{e} \sin^{-1} e \\ \alpha_0 = \beta_0 &= \frac{(1 - e^2)^{\frac{1}{2}}}{e^3} \sin^{-1} e - \frac{1 - e^2}{e^2} \\ \gamma_0 &= \frac{2}{e^2} - \frac{2(1 - e^2)^{\frac{1}{2}}}{e^3} \sin^{-1} e \\ e &= (1 - C^2/A^2)^{\frac{1}{2}}\end{aligned}\tag{2.5}$$

2. **Prolate** ($A > B = C$):

$$\begin{aligned}\chi_0 &= \frac{1}{e} \ln \frac{1 + e}{1 - e} \\ \alpha_0 &= \frac{1 - e^2}{e^3} \ln \frac{1 + e}{1 - e} - 2 \frac{1 - e^2}{e^2} \\ \beta_0 = \gamma_0 &= \frac{1}{e^2} - \frac{1 - e^2}{2e^3} \ln \frac{1 + e}{1 - e} \\ e &= (1 - C^2/A^2)^{\frac{1}{2}}\end{aligned}\tag{2.6}$$

2.2 Calculating the torque from potential

We start with the general solution for Φ_{int} of homogeneous ellipsoid (equation 3.1),

$$\Phi_{int} = \pi G \rho (\alpha_0 x^2 + \beta_0 y^2 + \gamma_0 z^2 - \chi_0)$$

Let the angle between major axis (A) of the ellipsoid and line joining the binary stars be $\Delta\phi$. The new coordinate system (x', y', z') is defined as,

$$\begin{bmatrix} x' \\ y' \\ z' \end{bmatrix} = \begin{bmatrix} \cos(\Delta\phi) & -\sin(\Delta\phi) & 0 \\ \sin(\Delta\phi) & \cos(\Delta\phi) & 0 \\ 0 & 0 & 1 \end{bmatrix} \begin{bmatrix} x \\ y \\ z \end{bmatrix} = \begin{bmatrix} x \cos(\Delta\phi) - y \sin(\Delta\phi) \\ x \sin(\Delta\phi) + y \cos(\Delta\phi) \\ z \end{bmatrix}$$

The equation for Φ_{int} in new coordinate system is,

$$\begin{aligned}
 \Phi_{int} &= \pi G \rho [\alpha_0(x')^2 + \beta_0(y')^2 + \gamma_0(z')^2 - \chi_0] \\
 &= \pi G \rho [\alpha_0\{x \cos(\Delta\phi) - y \sin(\Delta\phi)\}^2 + \beta_0\{x \sin(\Delta\phi) + y \cos(\Delta\phi)\}^2 + \gamma_0(z')^2 - \chi_0] \\
 &= \pi G \rho [x^2\{\alpha_0 \cos^2(\Delta\phi) + \beta_0 \sin^2(\Delta\phi)\} + xy \sin(2\Delta\phi)(\beta_0 - \alpha_0) \\
 &\quad + y^2\{\alpha_0 \sin^2(\Delta\phi) + \beta_0 \cos^2(\Delta\phi)\} + z^2\gamma_0 - \chi_0]
 \end{aligned} \tag{2.7}$$

Force can be calculated by taking the negative gradient of the potential,

$$\vec{F} = -m \nabla \Phi_{int} = -\pi G \rho m [\{2x(\alpha_0 \cos^2(\Delta\phi) + \beta_0 \sin^2(\Delta\phi)) + y \sin(2\Delta\phi)(\beta_0 - \alpha_0)\} \hat{i} \\
 + \{x \sin(2\Delta\phi)(\beta_0 - \alpha_0) + 2y(\alpha_0 \sin^2(\Delta\phi) + \beta_0 \cos^2(\Delta\phi))\} \hat{j} + 2\gamma_0 z \hat{k}] \tag{2.8}$$

Torque can be calculated by taking the cross product of position vector and Force vector.

$$\tau = \vec{r} \times \vec{F} = -\pi G \rho m \begin{pmatrix} \hat{i} & \hat{j} & \hat{k} \\ x & y & z \\ 2x(\alpha_0 \cos^2(\Delta\phi) + \beta_0 \sin^2(\Delta\phi)) & x \sin(2\Delta\phi)(\beta_0 - \alpha_0) & 2\gamma_0 z \\ +y \sin(2\Delta\phi)(\beta_0 - \alpha_0) & +2y(\alpha_0 \sin^2(\Delta\phi) + \beta_0 \cos^2(\Delta\phi)) & \end{pmatrix}$$

$$\begin{aligned}
 \tau &= \pi G \rho m [z\{x \sin(2\Delta\phi)(\beta_0 - \alpha_0) + 2y(\alpha_0 \sin^2(\Delta\phi) + \beta_0 \cos^2(\Delta\phi) - \gamma_0)\} \hat{i} \\
 &\quad - z\{2x(\alpha_0 \cos^2(\Delta\phi) + \beta_0 \sin^2(\Delta\phi) + \gamma_0) + y \sin(2\Delta\phi)(\beta_0 - \alpha_0)\} \hat{j} \\
 &\quad + \{\sin(2\Delta\phi)(\beta_0 - \alpha_0)(y^2 - x^2) + 2xy(\alpha_0 \cos(2\Delta\phi) - \beta_0 \cos(2\Delta\phi))\} \hat{k}]
 \end{aligned} \tag{2.9}$$

Furthermore, if we take the approximation that both the stars stay on orbital plane for the entire time ($z = 0$) and we take the binary axis on $y = 0$, we can further reduce the expression,

$$\tau = \tau_z = -\frac{1}{2}\pi GM (\beta_0 - \alpha_0) \cos(\Delta\phi) \sin(\Delta\phi) \rho a^2 \tag{2.10}$$

where a is the binary separation.

2.3 Binary Separation

In order to solve for the binary separation, we take an assumption that $\log_{10}(\rho a^2)$ and $\log_{10}(t)$ are linearly related.

$$\log_{10}(\rho a^2) = -p * \log_{10}(t) + q \quad (2.11)$$

Using the relation, we modify the expression for torque,

$$M \frac{d}{dt} \left(r^2 \frac{d\phi}{dt} \right) = -\frac{1}{2} \pi GM (\beta_0 - \alpha_0) \cos(\Delta\phi) \sin(\Delta\phi) 10^q \times t^{-p} \quad (2.12)$$

Solving the equation for a, we obtain the expression for binary separation.

$$a = 2 \left[\sqrt{\frac{a_0}{2}} + \frac{10^q \pi \sqrt{8G}}{3\sqrt{M}} (\beta_0 - \alpha_0) \cos(\Delta\phi) \sin(\Delta\phi) \left(\frac{1}{t^{p-1}} - \frac{1}{t_0^{p-1}} \right) \right]^2 \quad (2.13)$$

Chapter 3

Methods

We summarize the methods used to perform the analysis here.

3.1 AstroBEAR

The 3D simulation was performed by lc18, lc20 using the hydrodynamics code AstroBEAR [Cunningham et al., 2009, Carroll-Nellenback et al., 2013]. The code is designed for simulating both 2D and 3D multiphysics problems using Adaptive Mesh Refinement (AMR).

3.2 Simulation parameters

The primary star in our simulation is an Asymptotic Giant Branch (AGB) star with initial mass $M_1 = 1.78M_\odot$ and radius $R_1 = 61.1R_\odot$. The core mass of the primary ($M_{1,c} = 0.53M_\odot$) is equal to the mass of companion star. The initial parameters of the system is listed in 3.1.

Quantity	Symbol	Values for the run
Primary mass	M_1	$1.78M_\odot$
Core particle mass	$M_{1,c}$	$0.53M_\odot$
Envelope mass	$M_{1,e}$	$1.25M_\odot$
Secondary mass	M_2	$0.53M_\odot$
Primary radius	R_1	$61.1R_\odot$
Initial separation	a_i	$62.0R_\odot$
Softening Radius	r_{soft}	$2.4R_\odot$
Ambient density	ρ_{amb}	$1.0 \times 10^{-9} \text{ g cm}^{-3}$
Ambient pressure	P_{amb}	$1.0 \times 10^4 \text{ dynecm}^{-2}$

Table 3.1: Parameters of the simulation analysed in this work

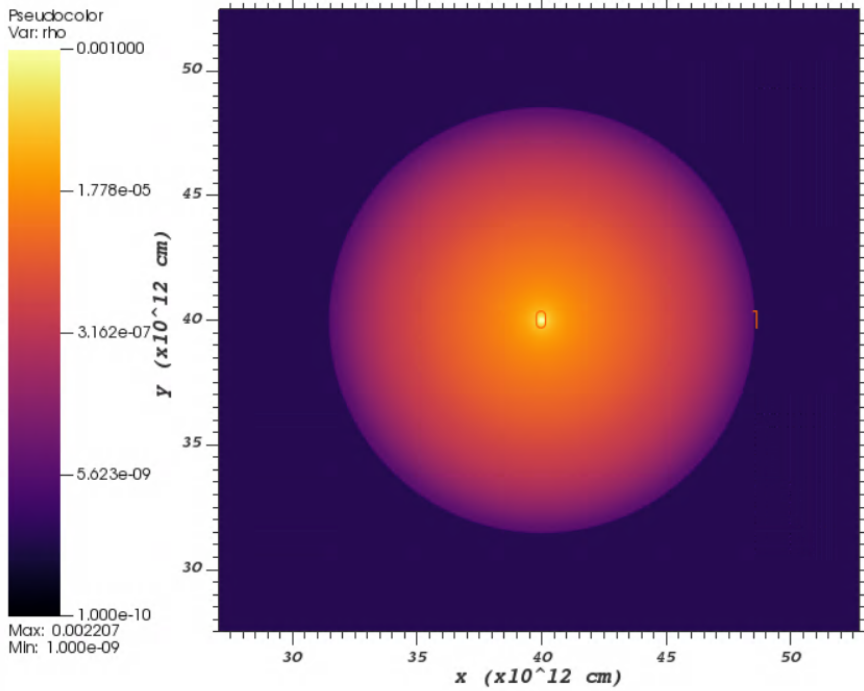


Figure 3.1: Gas density, ρ , in $g.cm^{-3}$ on orbital plane in the initial frame of the simulation in log-pseudocolor plot. The numbers 0 and 1 represent primary core and secondary, respectively.

The simulation domain is a cube with length $1150R_{\odot}$ where the primary core is placed at the center of the mesh. The AGB core and companion (hereafter referred as "particle 1" and "particle 2") has been modelled as point particles which interact with each other and gas with gravity only. AstroBEAR is capable of calculating the gravitational interaction between all three of particle-particle, particle-gas and gas-gas. The constant density (ρ_{amb}) and pressure (P_{amb}) of the ambient medium has been taken as $1.0 \times 10^{-9} \text{ g cm}^{-3}$ and $1.0 \times 10^4 \text{ dyne cm}^{-2}$, respectively. A spline function with constant softening radius (r_{soft}) R_{\odot} has been added to smoothen the particle potential [Springel, 2010]. The gravitational interaction outside and inside the softening radius are respectively Newtonian (for $r > r_{soft}$) and shallower than

Newtonian (for $r < r_{soft}$) [Ohlmann et al., 2017]. A varying softening radius has been studied in lc19b and its effect on drag force has been found out to be insignificant.

3.3 VisIt as an analysing tool

VisIt is an open-source, parallelized software for visualizing data defined on two and three-dimensional structured and unstructured meshes. VisIt works both on a graphical user interface (GUI) and a python based command prompt. The software has been extensively used in this work for visualization of the data, calculation and plotting.

3.4 Evolution of the system

The following density pseudocolor-contour plots at different time frames can help visualize the system. The density slices have been taken through orbital plane of the system and shows the density distribution as a function of time. The snaps have been taken from t [days] = 0.0, 23.1, 46.3, 69.4, 92.6, 115.7, 138.9, 162.3, 185.2, 208.3, 231.5 and 254.6.

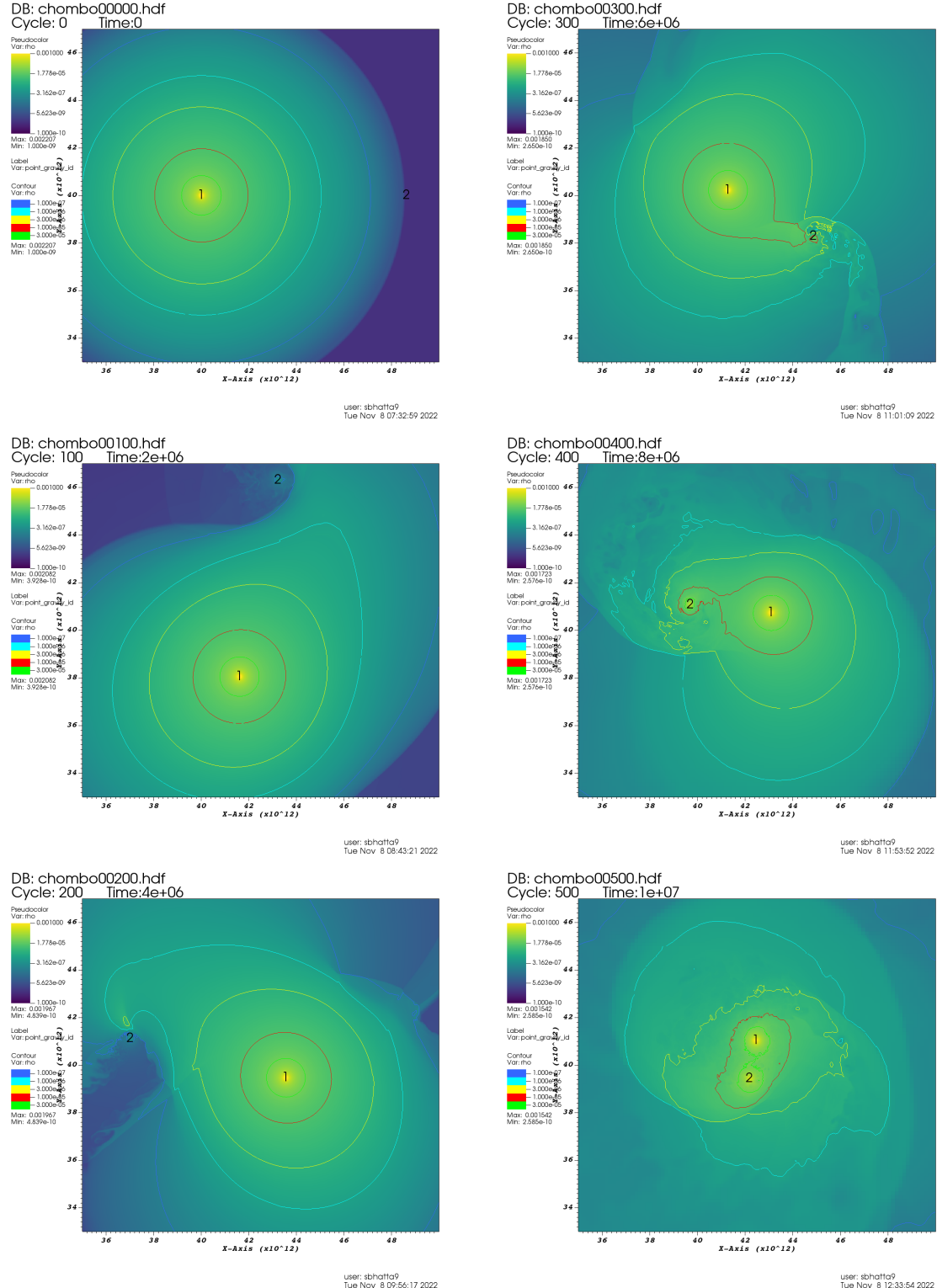


Figure 3.2: Pseudocolor-contour plot for gas density through orbital plane at t [d] = 0.0, 23.1, 46.3, 69.4, 92.6 and 115.7.

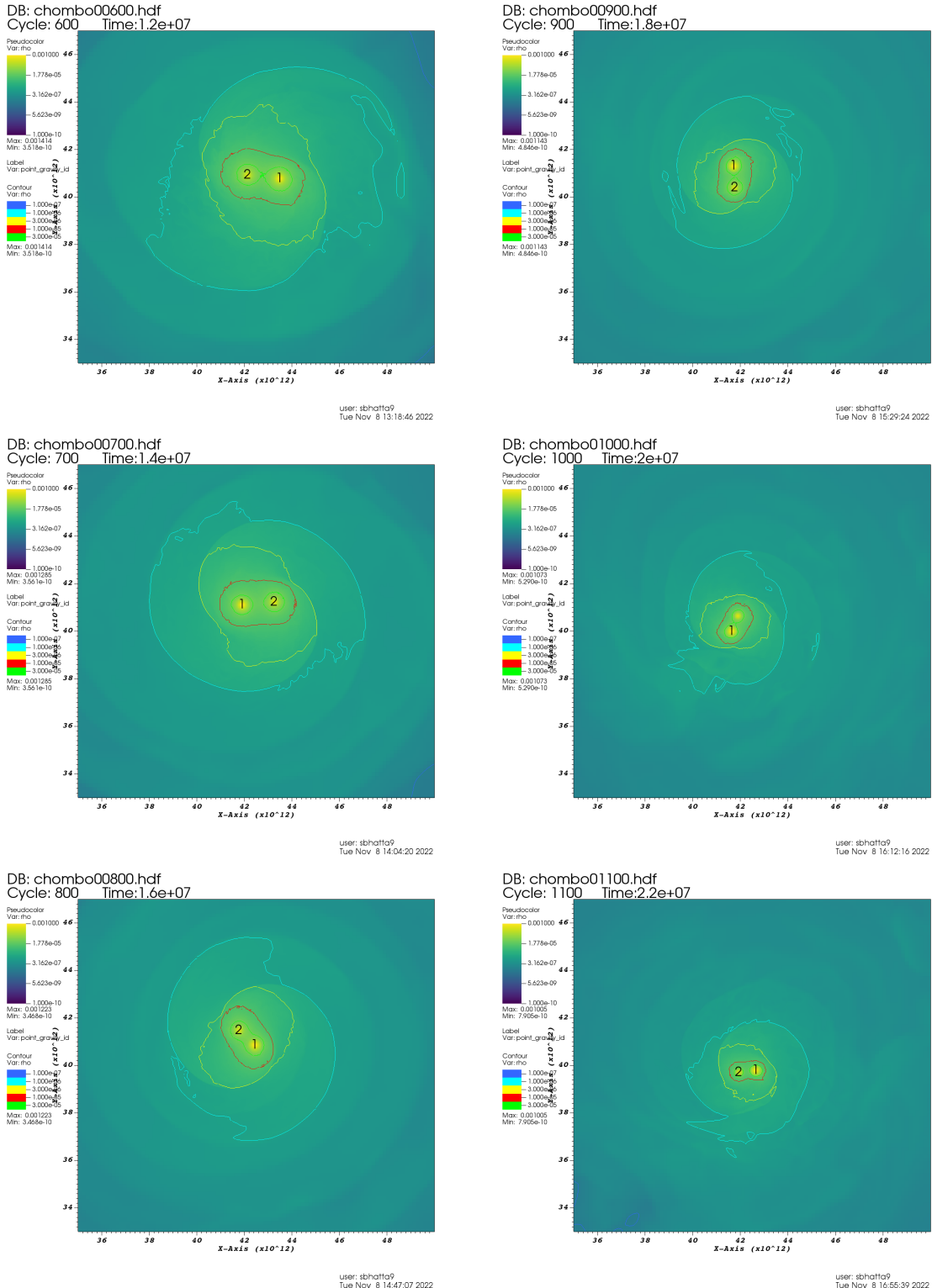


Figure 3.3: Pseudocolor-contour plot for gas density through orbital plane at t [d] = 138.9, 162.3, 185.2, 208.3, 231.5 and 254.6.

As we can observe, the simulation starts with a spherically symmetric primary star with a secondary star on its surface. There is an initial tidal overflow of gas from particle 1 to particle 2. During the first periastron passage at ~ 70 days, particle 2 first comes closer to being inside a same density contour. As the star again moves away, the envelope can't sustain its shape and the star goes out of the envelope with a bulge of gas at its trail. The sixth frame at 115.7 days is the first frame with a noticeable common envelope.

Chapter 4

Results and Discussion

4.1 Orbital Separation

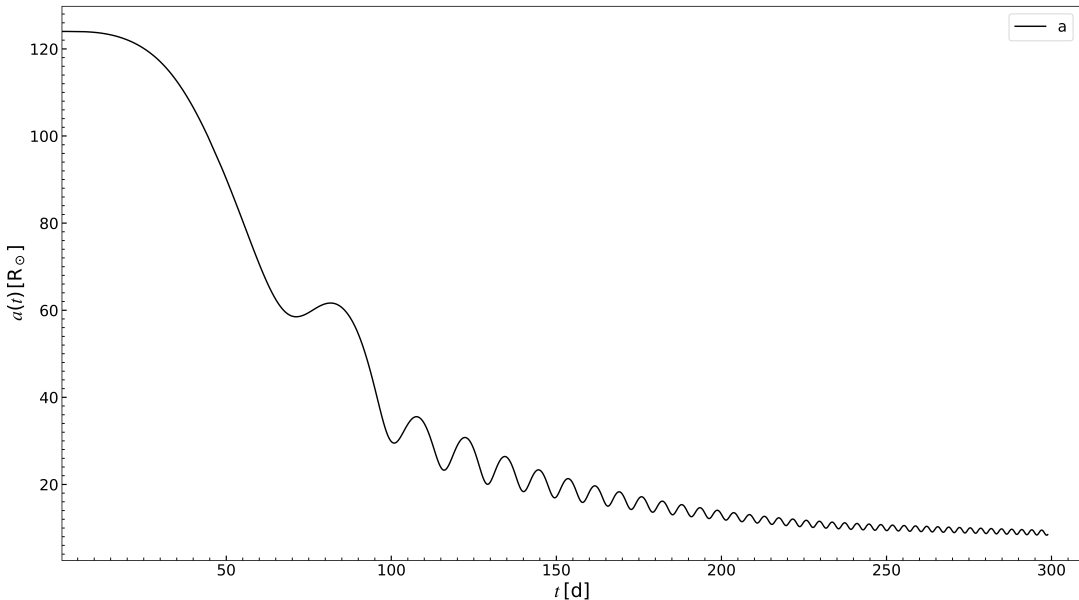


Figure 4.1: Separation between two particle cores in orbital plane as a function of time

Figure 4.1 shows the inter-particle separation in orbital plane as a function of time. The plunge-in phase or the initial reduction in orbital separation continues till ~ 70 days. Compared to previous runs by [Chamandy et al. \[2018\]](#), [Chamandy et al. \[2020\]](#), the system takes longer to reach its first periastron passage (the first local minima of orbital separation), owing to its lower companion mass. The orbit gains a periodic nature after second periastron passage, however, it still doesn't reach a stationary orbit by the end of the simulation. The time-averaged orbital separation and period

of the orbit both keep decreasing with time.

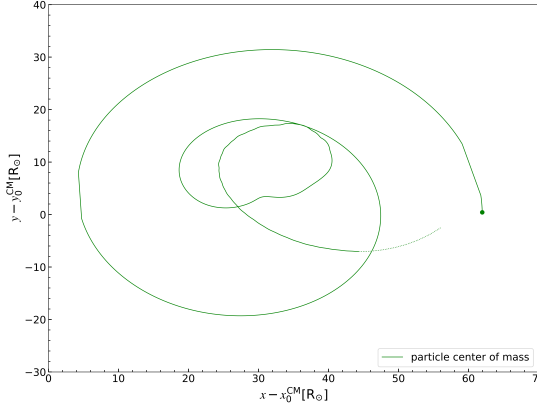


Figure 4.2: Motion of the center of mass of the particle cores in orbital plane

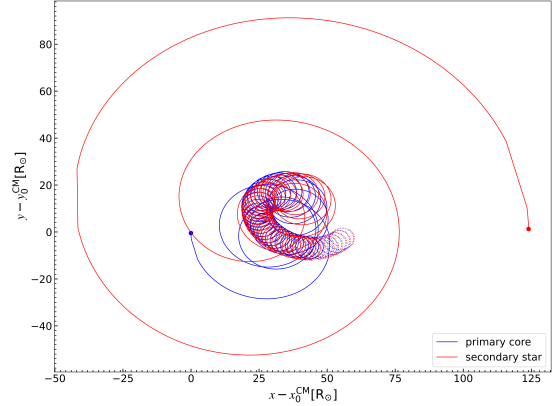


Figure 4.3: Orbit of particle cores in orbital plane

Figure 4.2 illustrates the motion of the center of mass of the particle cores in orbital plane. The units of the axes are in solar radii. The shift in center of mass from origin is caused by the gravitational interaction between gas and particle 2 and is a notable phenomena in common envelope evolution. Many of the bipolar PNe with a binary system at the nucleus shows a shifted center of mass in the orbital plane of the system, this is supposedly caused by companion-gas interaction at some stage of binary evolution.

The orbit of the particles throughout the simulation is shown in figure 4.3. The primary is shown in blue color, and it's located at the origin at the beginning of the simulation. The secondary, shown in color red, starts from the edge of the primary star and spirals inwards. Both the axes have units denoted in solar radii.

4.2 Drag Force Evolution

We compute the gravitational force between particle and gas by integrating the force per unit volume for each particle.

$$\mathbf{F}_{1-\text{gas}} = GM_{1,c} \sum_V \rho(s) \left[(s - s_{1,c}) / |s - s_{1,c}|^3 \right] d^3s \quad (4.1)$$

$$\mathbf{F}_{2-\text{gas}} = GM_2 \sum_V \rho(s) \left[(s - s_2) / |s - s_2|^3 \right] d^3s \quad (4.2)$$

Here gravitational interaction between particle and gas is calculated in lab frame, where G is universal gravitational constant, $M_{1,c}$ and M_2 are the masses of primary core and secondary, respectively, V is the total volume of the simulation domain, $\rho(s)$ is the gas density at position s , $S_{1,c}$ and s_2 are positions of primary core and secondary star, respectively.

We further calculate the drag force on particle 2 in the non-rotating, non-inertial rest frame of particle 1 in order to compare with theory and previous results,

$$\mathbf{F}_{2-\text{gas},1} = \mathbf{F}_{2-\text{gas}} - (M_2/M_{1,c}) \mathbf{F}_{1-\text{gas}} \quad (4.3)$$

The 1 after $\mathbf{F}_{2-\text{gas}}$ denotes the reference frame. The gravitational interaction between particles has been ignored in the equation, as we are only concerned about the dynamical friction force exerted by the gas. We also calculate the ϕ component of force $[(\mathbf{s}_2 - \mathbf{s}_1) \times \mathbf{F}_{2-\text{gas},1}/a \cdot \hat{\mathbf{z}}]$ and force along velocity component $[F_{2-\text{gas},1} \cdot (v_2 - v_1) / |v_2 - v_1|]$

The drag force on particle 2 as a function of time is plotted in figure 4.4 with results from [Chamandy et al. \[2020\]](#) added for comparison. The black solid line shows the azimuthal component of the drag force on particle 2 in units of 10^{33} dyne in rest frame of particle 1. The darkgrey and gold dashed lines represent the azimuthal component

in lab frame and component along relative velocity in frame of particle 1. The orbital separation between the core is plotted on the right axis in units of solar radius.

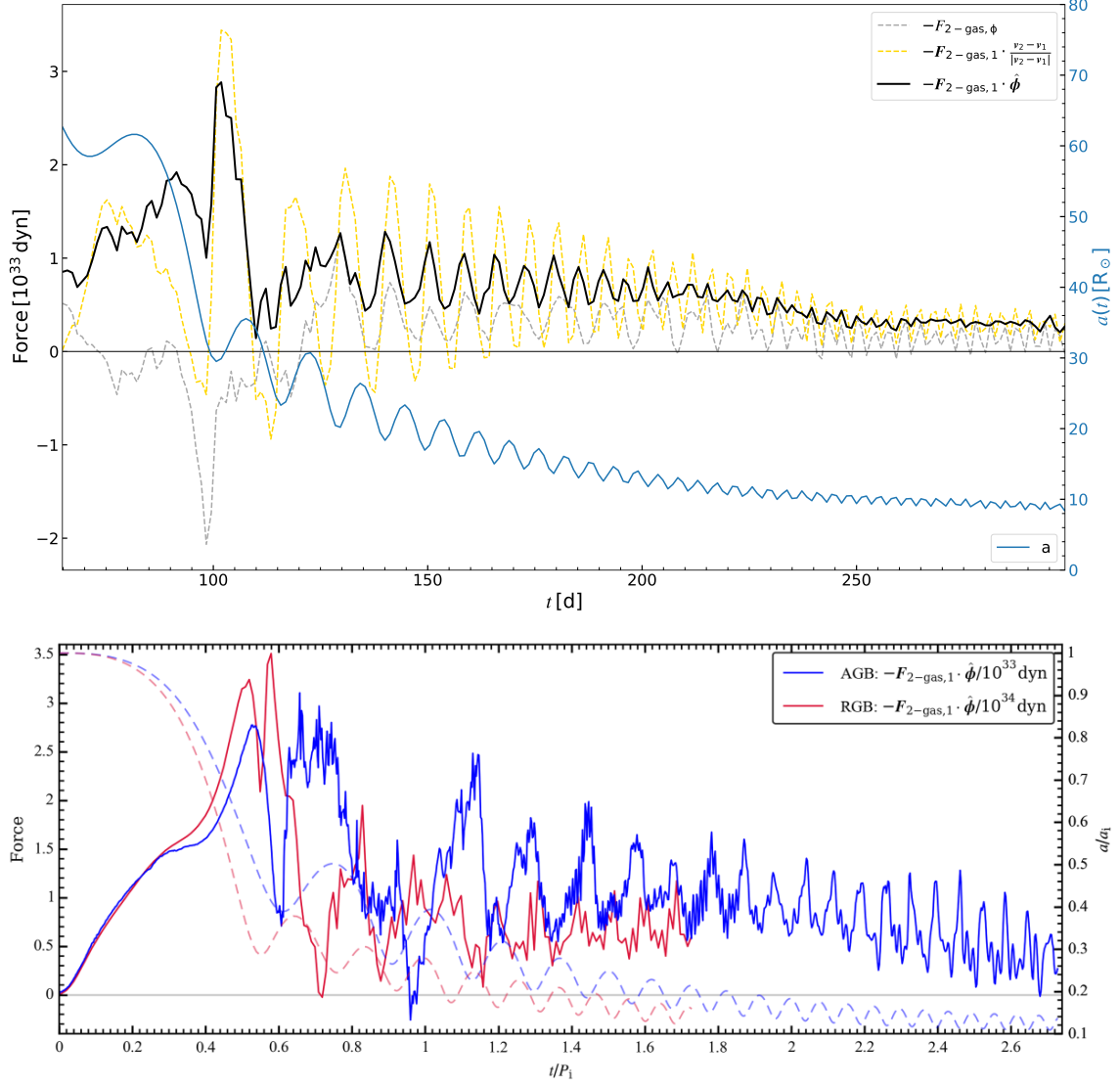


Figure 4.4: Top: (i) The ϕ component of drag force in lab frame is plotted in dark-grey dashed line; (ii) The force along velocity component is plotted in gold dashed line; (iii) The azimuthal component of the drag force on particle 2 in rest frame of particle 1 is plotted in black solid line; (iv) The orbital separation is plotted on the right axis as a reference. Bottom: Results from [Chamandy et al. \[2020\]](#), which calculates the azimuthal component of drag force in rest frame of particle 1 for an AGB and a RGB primary core star (Courtesy: [Chamandy et al. \[2020\]](#))

The bottom figure is taken from [Chamandy et al. \[2020\]](#), who compares the drag force computed for an AGB and a RGB core. The blue line shows the azimuthal component of drag on particle 2 for an AGB core as primary with initial parameters, $M_1 = 1.78M_\odot$, $M_{1,c} = 0.53M_\odot$ and $M_2 = 1.98M_\odot$. The red line shows the same for a RGB core system with $M_1 = 1.96M_\odot$, $M_{1,c} = 0.37M_\odot$ and $M_2 = 1.98M_\odot$. The magnitude of force observed for the RBG core system is an order higher than than the AGB systems, while the AGB systems with two different initial parameters are in good agreement in terms of magnitude of the force at maximum values.

In all three cases, the ϕ component reaches its maximum magnitude around second periastron passage (~ 100 days in our system) and falls to nearly zero right after that. After that, the force quickly adapts to follow a periodic pattern, in resonance with the orbital period. We can see that an increased separation between the stars decreases the magnitude of drag force. This can be explained via the process of accretion by particle 1. As the secondary starts gaining mass from the primary and the primary starts losing mass, it also loses its spherical symmetry and starts having bulge of material behind its direction of motion. So, when the stars come closer to each other, the secondary experiences a gravitational pull along its direction of motion; the bulge of material behind star 1 actually applies a 'thrust', opposing the overall 'drag'.

As discussed in 1, we have also found that theory and simulation are in better match in intermediate time scales ($R_a < H_\rho$) than early or late times. Note that the force is plotted in 4.4 (top) is from a later time frame ($t = \sim 65$ days, right before first periastron passage).

4.3 Evolution of Torque

Total torque applied on both the particles is calculated about their center of mass with two different methods. First we compute the torque from the calculated drag force, obtained by performing an integration over whole of simulation domain. The torques from fictitious forces from shift in center of mass cancels out and we are left with,

$$\tau_z = \frac{M_2}{M_{1,c} + M_2} a F_{1-\text{gas},\phi} + \frac{M_{1,c}}{M_{1,c} + M_2} a F_{2-\text{gas},\phi} \quad (4.4)$$

After that, we calculate the rate of change in angular momentum of the particles and find that is in good agreement with the torque calculated from force.

$$J_{1-2,z} = M_{1,c} [(\mathbf{s}_1 - \mathbf{s}_{CM}) \times (\mathbf{v}_1 - \mathbf{v}_{CM})]_z + M_2 [(\mathbf{s}_2 - \mathbf{s}_{CM}) \times (\mathbf{v}_2 - \mathbf{v}_{CM})]_z \quad (4.5)$$

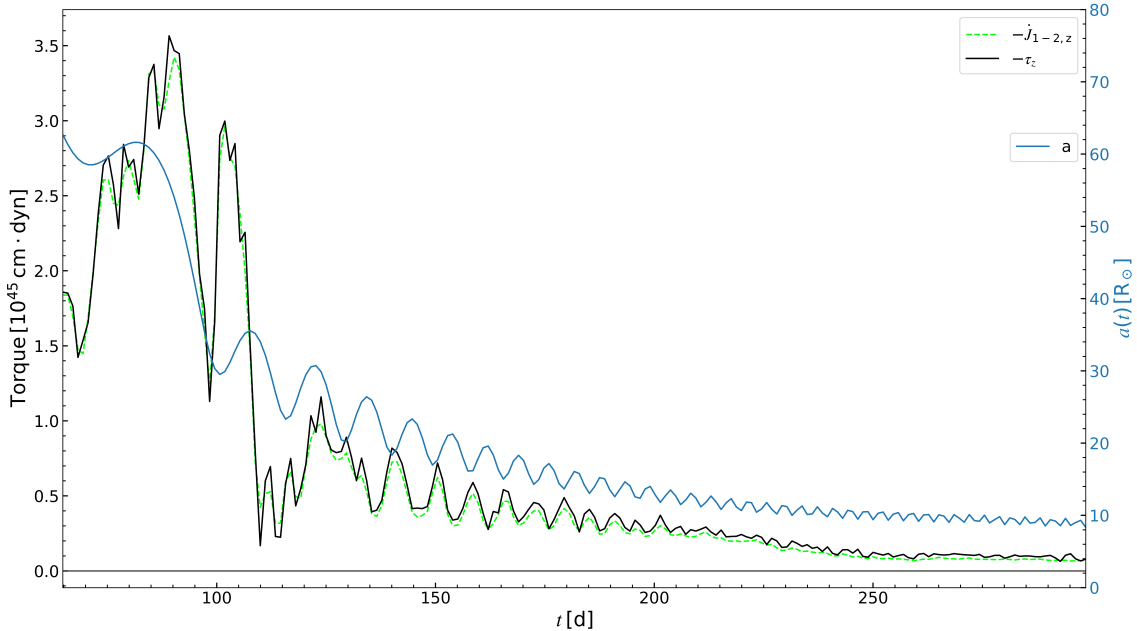


Figure 4.5: The z-component of torque calculated from force and orbital angular momentum has been plotted in solid black line and yellow dashed line, respectively. Orbital separation has been plotted on the right y-axis.

Figure 4.5 shows the z component of total torque applied on both particles, calculated from two different methods. Solid black line shows the calculated value from force (equation 4.4), while yellow dashed line shows the value calculated from orbital angular momentum (equation 4.5). The calculated torque from both methods, being in good agreement is a validation of the calculated force. As expected, we observe a relation between orbital separation and total torque, similar to force plot.

4.4 Selection of Ellipsoidal Surface

Since our goal is to model the torque of late times as a function of time, it is important to define what we consider to be "late time". Based on our observations from the simulation, we have noticed that the equidensity surfaces of gas take on an ellipsoidal shape after approximately 115 days (the 500th frame in the simulation). After this point, the orbital separation, force, and torque also vary periodically, in a less dramatic manner. Therefore, we will begin our analysis from the 500th frame (115 days) and continue until the end of the simulation (approximately 300 days).

Once we have established the time domain, the next step is to identify the equidensity surface that contributes significantly to the torque. To accomplish this, we calculate the ratio of the torque applied by a certain amount of gas, denoted by τ , to the total torque applied by all the gas, denoted by τ_0 , on the particles. We use the parameter ρ/ρ_{max} to define the amount of gas, where ρ is the density of the surface of the ellipsoid under consideration and ρ_{max} is the maximum density present in the time frame (which is typically the density near the star's surface).

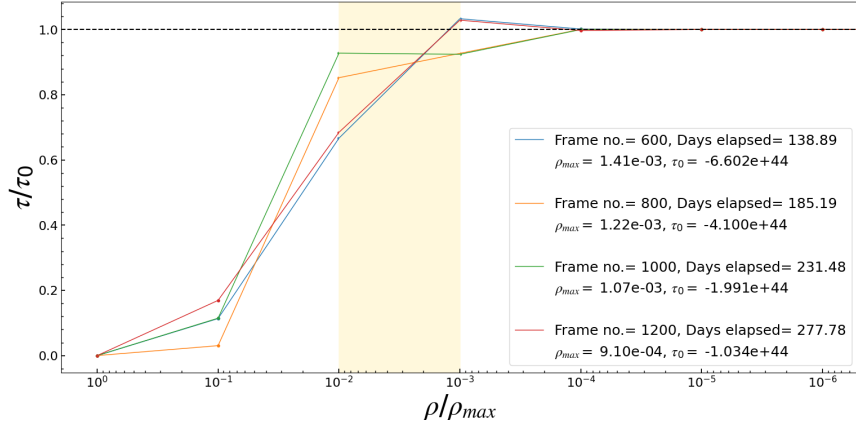


Figure 4.6: Ratio of torque exerted on the binary system by some amount of gas and all of gas is plotted for different frames from the simulation is shown.

We begin by plotting the ratio τ/τ_0 as a function of ρ/ρ_{max} for different time frames. We observe that the region which contributes to nearly all of the torque is between 10^{-3} and 10^{-2} (corresponding to 0.1% and 1%, respectively). We then vary the percentage within this range and plot τ and τ/τ_0 as a function of time. We find that the curve for $\rho/\rho_{max} = 0.6\%$ is the least deviated from $\tau = \tau_0$.

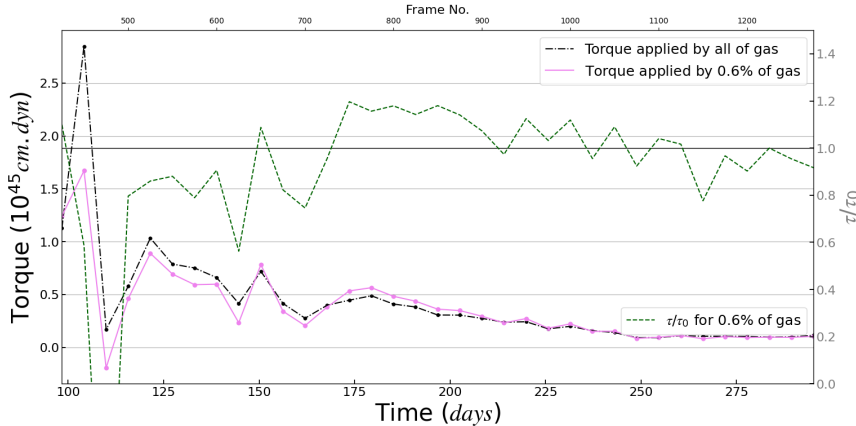


Figure 4.7: The left y-axis of the plot shows the torque as a function of time. The torque applied by all of the gas is represented by the black dashed line, while the torque applied by a certain percentage of gas is shown in blue. On the right y-axis, we display the ratio of both the torques.

We plot the same for different values of ρ/ρ_{max} and find out that the curve for

0.6% is the least deviated one from $\tau = \tau_0$ (black solid line in figure 4.2).

4.5 Fitting the Ellipsoids

Once we have identified the equidensity surface that contributes significantly to the torque, we need to parameterize the ellipsoid that represents the surface. We use A to denote the semi-major axis, and B and C to denote the semi-minor axes in the orbital and perpendicular planes, respectively. We also need another parameter, $\Delta\phi$, to account for the lag between the binary system axis and the major axis of the envelope. However, we faced a challenge in VisIt, the analysis software we are using, which does not allow us to save the contour points for a 3-dimensional figure. Therefore, we had to fit the orbital and perpendicular planes separately.

First, we fit the three parameters, A, B and $\Delta\phi$ in orbital plane. We define the coordinates of the orbital plane such that the stars move on XY plane ($z=0$), with $y=0$ as the axis of the binary and origin as the center of mass of the stars. After fitting these three parameters, we rotate the axis of the binary by the angle $\Delta\phi$ (fitted from orbital plane) and take a perpendicular slice. This slice now contains the ellipse which has semi-axes A and C. We fix A from fitting of the orbital frame and then fit C.

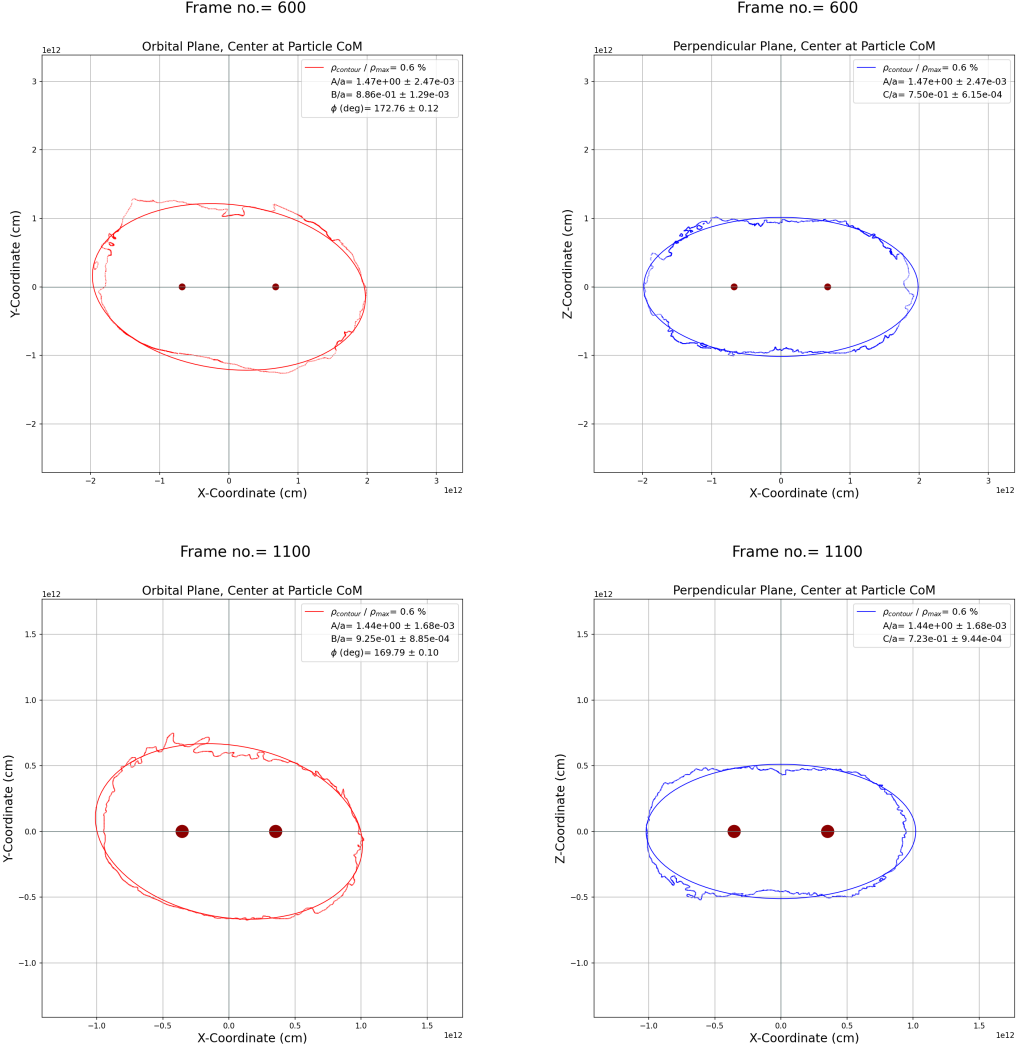


Figure 4.8: The contours of ellipses and fitted ellipses for orbital plane (left) and perpendicular plane (right) are shown for two different time-frames.

4.6 Parameter Evolution

After fitting the parameters A, B, C, and $\Delta\phi$, we proceed to analyze their evolution over time. To ensure the robustness of the trends, the ratios are plotted for three different values of ρ/ρ_{max} . In the following figure 4.9-4.15, the actual fitted values and Savitzky-Golay filtered smoothed trends are shown.

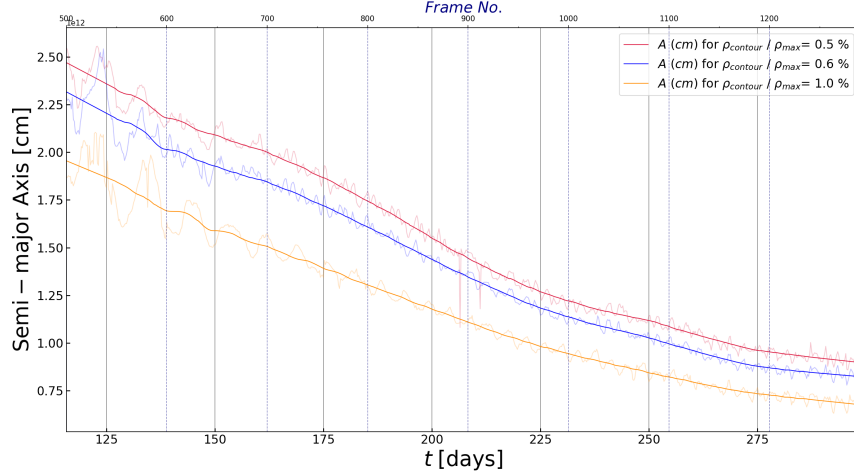


Figure 4.9: Evolution of semi-major axis (A) with time.

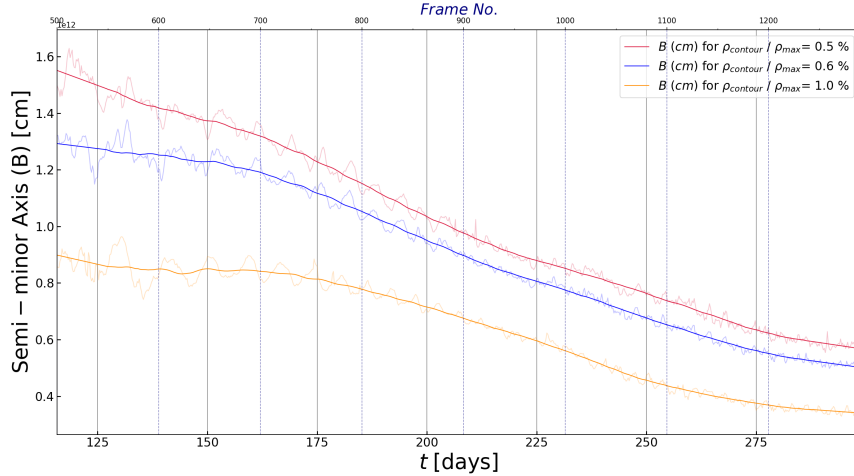


Figure 4.10: Evolution of semi-minor axis in orbital plane (B) with time.

We can use the parameter values in equation 3.9 and get the torque for each time frame. However, we must remember that our final goal is to build the time-dependant model of torque as simple and universal as possible. In order to do so, we choose the following parameters, A/a , B/A , C/A (a = orbital separation) as they are expected to have less dependence on the initial mass and category of the star. Please note that

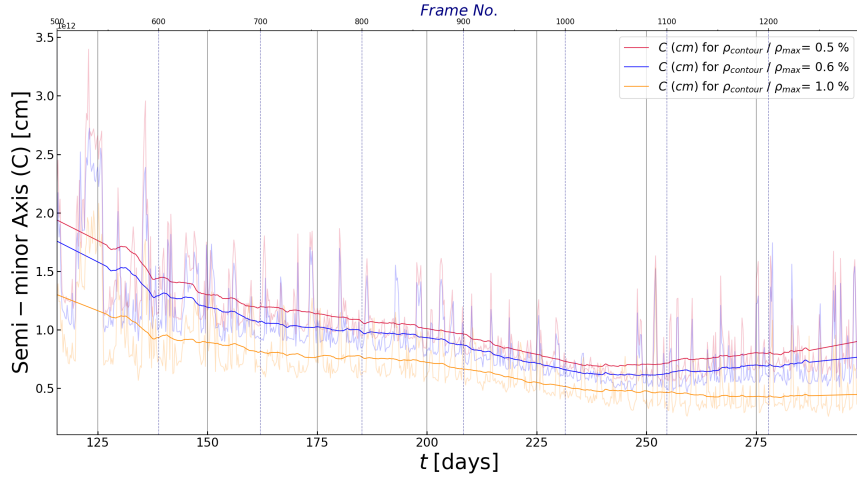


Figure 4.11: Evolution of semi-minor axis in perpendicular plane (C) with time.

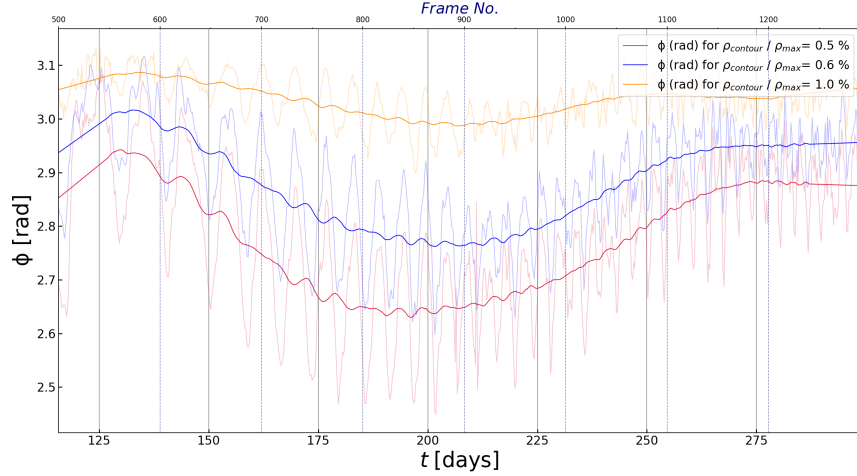


Figure 4.12: Evolution of lag between binary axis and major axis of the ellipsoid ($\Delta\phi$) with time.

the mass ratio of the stars, however, would still be a determining factor for the shape of the ellipsoid (or in more general terms, the shape of the equidensity surface we are fitting). In any case, we start developing our model with the simplest case of two stars, both having equal core mass.

The figures show the time evolution of three ratios, A/a , B/A and C/A , where a

is the semi-major axis of the binary system. The dashed line in each figure represents the approximation of taking each ratio as a linear function of time, while the dotted line shows the ratio as the average of all values. In following sections, the impact of these approximations on the time-dependent torque model is evaluated.

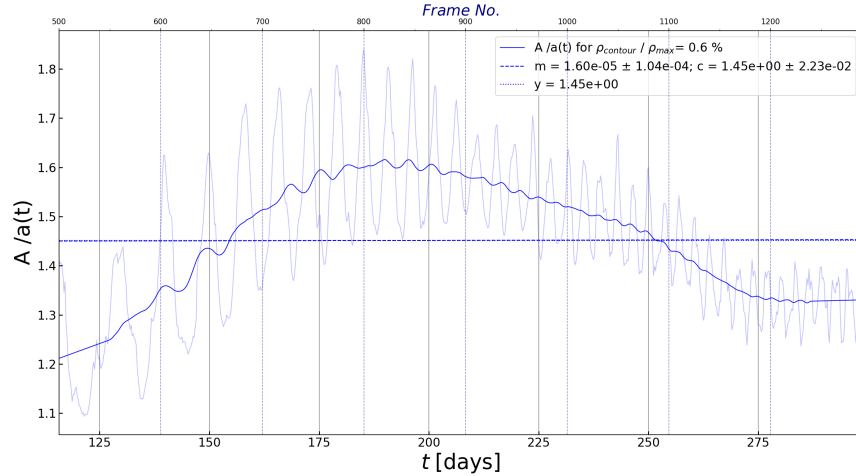


Figure 4.13: Evolution of the ratio A/a with time.

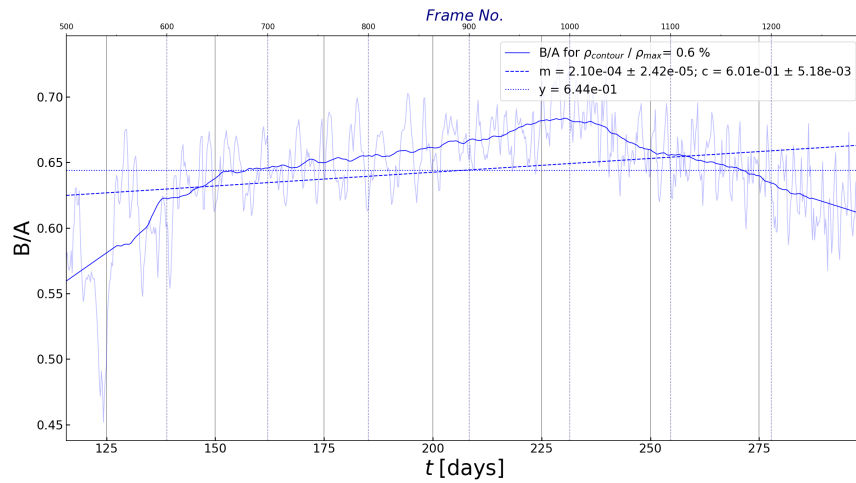


Figure 4.14: Evolution of the ratio B/A with time.

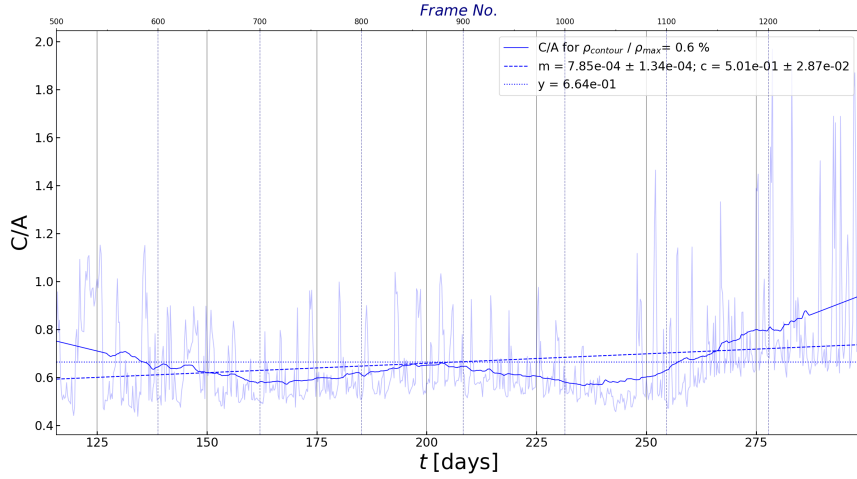


Figure 4.15: Evolution of the ratio C/A with time.

4.7 The Time-Dependant Model of Torque

4.7.1 Taking the approximation of a prolate ellipsoid case

A prolate ellipsoid is defined as the case where both the semi-minor axes are equal in magnitude ($A > B = C$). This approximation was used by [Escala et al. \[2004\]](#) in his case of binary systems with supermassive black holes instead of stars. We plot the ratio C/B with time to verify if this approximation is a valid one for our case.

As we can observe from the figure 4.16, the ratio is not constant throughout time. However, the average of the ratio is 1.04, which is close to 1. Also, the magnitude of the ratio varies only between 0.85 and 1.5, keeping the variance low. Moreover, we refer to equation 3.6 to show how simplified the constants α_0 , β_0 , γ_0 and χ_0 becomes when compared to the general case of $A > B > C$ (equation 3.2). Also, in the prolate case, the constants can only be represented using one parameter, eccentricity (e), which is a function of just C/A ($B = C$).

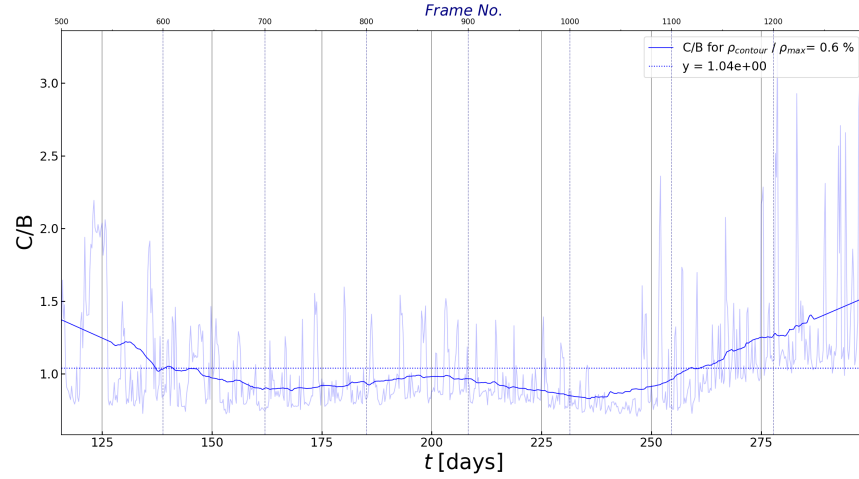


Figure 4.16: Time evolution of the ratio C/B .

4.7.2 Modelling the torque

We calculate the torque using equation 2.10 and plot the z-component of torque to match with the previously calculated result.

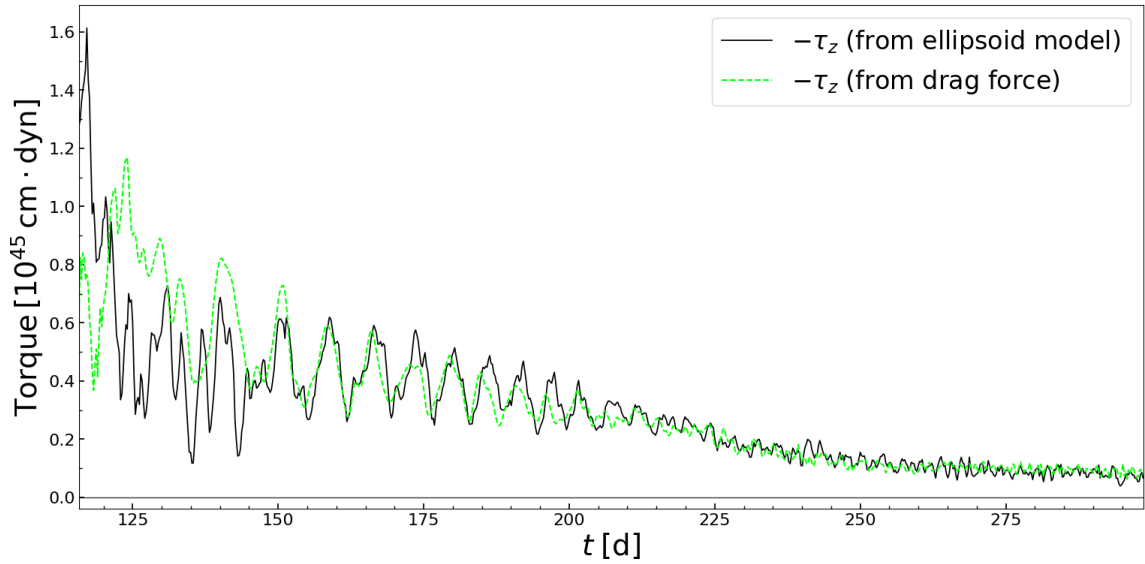


Figure 4.17: The torque has been calculated in two different methods. The solid black line shows the torque calculated from this homogeneous ellipsoid model (equation 2.10) and the dashed gold line shows the torque calculated from drag force.

We can see from figure 4.17 that the model predicted torque is closely matching with the torque calculated previously. However, the model is currently using parameters which are fitted for every time frame. In order to build our model for a more generalised purpose, we can further use the parameters ρ_{mean} , a (orbital separation), C/A and $\Delta\phi$ as analytical functions of time and see how that approximation affects the result.

We choose C/A and $\Delta\phi$ constant with time and find that $C/A = 0.664$ and $\Delta\phi = 0.25 \text{ rad}$. We take these approximations and check how that affects the model.

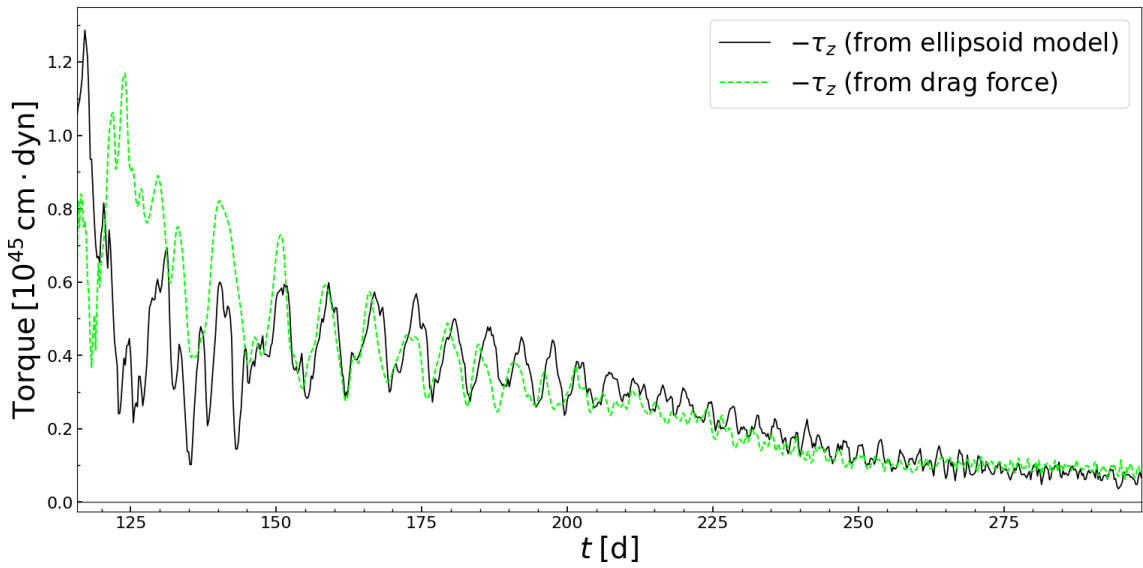


Figure 4.18: The torque has been calculated from the homogeneous ellipsoid model with the approximation $C/A = 0.664$

As we can observe from figure 4.18, the first approximation does not change the torque in any considerable way, but the approximation of lag angle adds a certain periodicity in the modelled torque and also deviates noticeably from the torque obtained from integrating the drag force. Nevertheless, the torque calculated from model with approximations still predicts the torque at late times with a high accuracy.

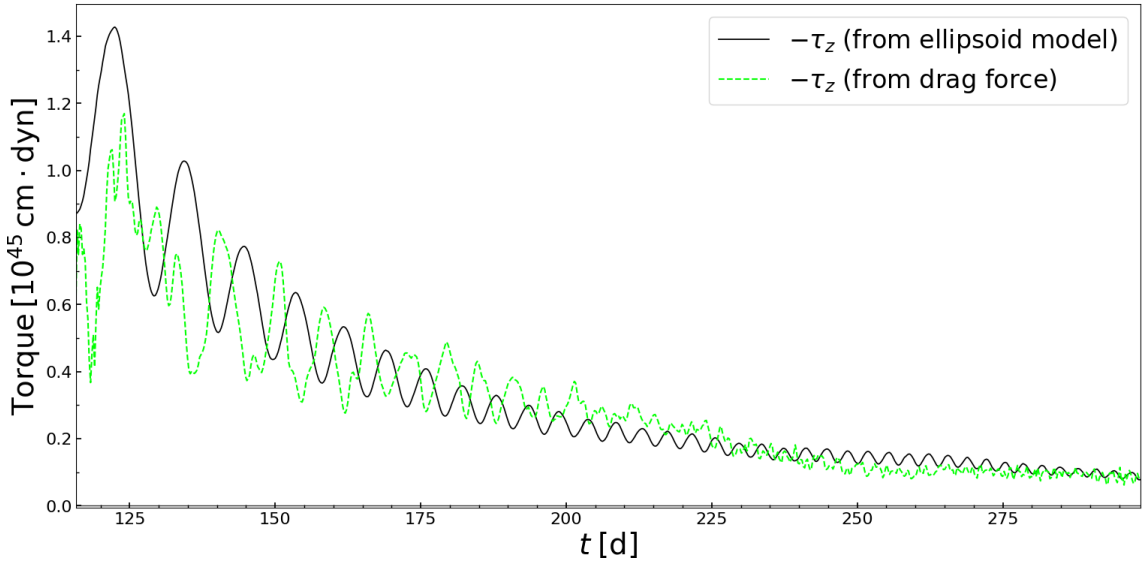


Figure 4.19: The torque has been calculated from the homogeneous ellipsoid model with the approximations $C/A = 0.664$ and $\Delta\phi = 25 \text{ rad}$.

4.8 Modelling the binary separation

We calculate the torque using equation 2.13 and get the values of p , q by fitting.

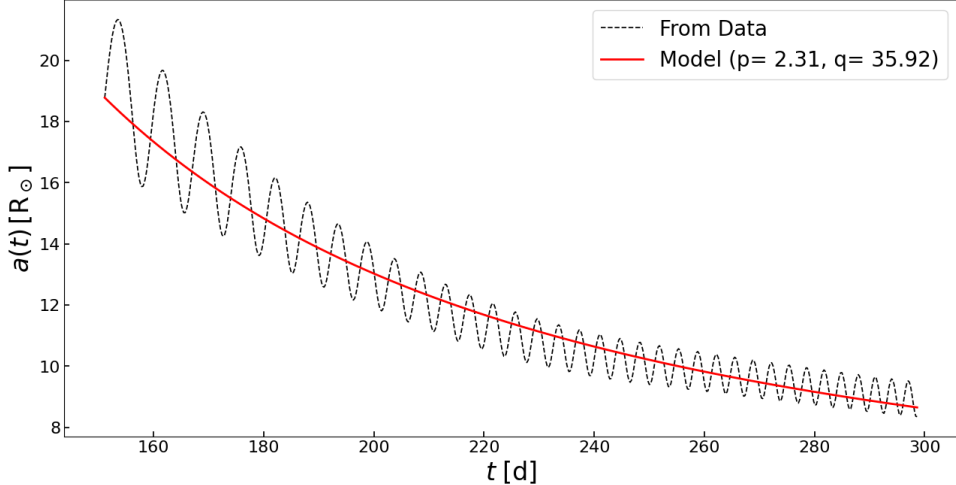


Figure 4.20: The black dashed line and red solid line are respectively the actual separation from simulation and the separation from model.

Chapter 5

Summary and Conclusions

A global CE evolution with an asymptotic giant branch (AGB) star as the primary star is analysed in this work. The secondary star in this simulation has the same mass as primary core and is situated at the outer radius of the AGB at the beginning of the simulation. The simulation evolves for ~ 40 orbital revolutions and we find out that:

- The center of mass of the system fails to reach a stationary orbit by the end of the time domain of the simulation, i.e. the energy transfer (from the core of the star to the gaseous medium) hasn't reached a stable stage of evolution.
- The drag force exerted on particle 2 by gas in the rest frame of particle 1 is in the order of 10^{33} (dyn). This value is of the same order as of the mass of primary, which is consistent with previous analysis.
- The total torque applied on the system by gas is calculated from drag force and change in angular momentum and the results compliment each other. It has been found in order of 10^{45} ($dyn.cm$) in early to intermediate stages and 10^{44} ($dyn.cm$) in later stages.

As we move on to build the model for the torque as a function of time, i.e. modelling the torque irrespective of integrating the force generated by whole of gas, we need to find out the amount of gas which accounts for almost all of the torque. In order to find out that, we use the parameter ρ/ρ_{max} to define the amount of gas, where ρ is the density of the surface of the ellipsoid under consideration and ρ_{max}

is the maximum density present in the time frame. We calculate the ratio of torque exerted by that much amount of the gas (τ) and total torque on stars (τ_0). It has been found out that the torque generated by the ellipsoid with surface density 0.6% of ρ_{max} contributes to almost all of it.

After getting the surface of the ellipsoid, we formulate the equation for torque from potential energy of the ellipsoidal body. In order to do so, we take two assumptions, the potential inside the ellipsoidal surface is represented as the potential inside a homogeneous ellipsoid of mean density and the ellipsoid considered a prolate one, i.e. the semi-major axes in both orbital and perpendicular plane are equal.

- We then fit the ellipsoidal surface, we obtain the parameters of the semi-axes (A, B, C) and the lag between the binary system axis and the major axis of the envelope ($\Delta\phi$).
- The parameter values of $C/A (= B/A)$ and $\Delta\phi$ are used to calculate the torque in each frame. It has been found that the calculated torque is in good agreement with the torque calculated from integrating the force from each gas particle.
- To further generalize the results, we use constant values of $C/A (= B/A)$ and $\Delta\phi$ to find that the model is still able to predict the torque in late times with good accuracy.
- We further develop a model for the binary separation with an assumption that the factor ρa^2 in the expression for torque decreases logarithmic-ally with time. We get the relation between the two by fitting expression 2.13 with the separation curve.

The origin of the torque exerted on stars during late times is a topic of debate within the scientific community. The objective of this thesis is to provide an explanation for this torque, and it successfully accomplishes this goal through the use of the homogeneous ellipsoid model. However, we can further enhance the model by eliminating the assumptions made during its construction.

The results obtained for binary separation can be extrapolated to future times beyond the simulation time domain. However, it should be noted that obtaining a good fit does not guarantee its applicability in the future, as the fitting parameters may change if the system undergoes a shift in its evolutionary path. Nonetheless, the expression for separation is derived from a physical model and provides a superior fit compared to other empirical functions like polynomials, exponentials, or Gaussians. The model for separation can also be enhanced by incorporating a more precise (or improved) relationship between density profile and time.

A potential avenue for further research involves extending the separation relation to a future time when the orbit stabilizes, and concurrently determining the efficiency parameter, α , within the energy formalism used to characterize the energy transfer during the common envelope phase.

Appendix A

Potential of Homoeoids and Ellipsoids

Definition. A homoeoid is a shell bounded by two concentric, similar ellipses in 2D or ellipsoids in 3D.

NEWTON'S THEOREM. *The attraction at any internal point of a homogeneous homoeoid is zero.*

COROLLARY. *Gravitational potential inside a homoeoid is constant throughout the interior.*

We take the center of the homoeoid and calculate potential there. The calculated potential (Φ_{int}) will be equal at any point inside the shell. The semi-axes of the bigger and smaller ellipsoids are denoted by A, B, C and mA, mB, mC , respectively, with $0 < m < 1$. If r_2 and r_1 are the radii of the two surfaces, then $r_1 = mr_2$. Taking an elementary cone with solid angle $d\omega$ at the center, we can calculate the contribution to potential from the frustum of the cone by,

$$\begin{aligned} d\Phi_{int} &= -G \int_{r_1}^{r_2} \rho r d\omega dr \\ &= -\frac{1}{2} G\rho (r_2^2 - r_1^2) d\omega \\ &= -\frac{1}{2} G\rho r_2^2 (1 - m^2) d\omega \end{aligned} \tag{5.1}$$

We integrate over ω to get Φ_{int} .

$$\Phi_{int} = -\frac{1}{2}G\rho(1-m^2) \int_S r^2 d\omega \quad (5.2)$$

Now we proceed to calculate the surface integral $\int_S r^2 d\omega$. In Cartesian coordinates, the equation of surface is given by,

$$\frac{x^2}{A^2} + \frac{y^2}{B^2} + \frac{z^2}{C^2} = 1$$

In polar coordinates,

$$\frac{1}{r^2} = \frac{\cos^2 \theta}{C^2} + \sin^2 \theta \left(\frac{\cos^2 \phi}{A^2} + \frac{\sin^2 \phi}{B^2} \right) \quad (5.3)$$

Putting r^2 in the surface integral,

$$\begin{aligned} \int_S r^2 d\omega &= \int_{\phi=0}^{2\pi} \int_{\theta=0}^{\pi} r^2 \sin \theta d\theta d\phi \\ &= 8 \int_0^{\pi/2} \int_0^{\pi/2} \frac{\sin \theta d\theta d\phi}{\cos^2 \theta / C^2 + \sin^2 \theta \left(\frac{\cos^2 \phi}{A^2} + \frac{\sin^2 \phi}{B^2} \right)} \end{aligned}$$

substituting $t = \tan \phi$ and $dt = \sec^2 \phi d\phi$,

$$\begin{aligned} \int_S r^2 d\omega &= 8 \int_0^{\pi/2} \int_0^{\infty} \frac{\sin \theta d\theta \sec^2 \phi d\phi}{\cos^2 \theta (1 + \tan^2 \phi) / C^2 + \sin^2 \theta / A^2 + \sin^2 \theta \tan^2 \phi / B^2} \\ &= 8 \int_0^{\pi/2} \int_0^{\infty} \frac{\sin \theta d\theta dt}{\sin^2 \theta / A^2 + \cos^2 \theta / C^2 + t^2 (\cos^2 \theta / C^2 + \sin^2 \theta / B^2)} \\ &= 8 \int_0^{\pi/2} \sin \theta d\theta \left[\frac{\tan^{-1} \left(\sqrt{\kappa_2 / \kappa_1} t \right)}{\sqrt{\kappa_1 \kappa_2}} \right]_0^{\infty} \\ &= 8 \int_0^{\pi/2} \sin \theta d\theta \frac{\pi}{2\sqrt{\kappa_1 \kappa_2}} \end{aligned}$$

where $\kappa_1 = \sin^2 \theta / A^2 + \cos^2 \theta / C^2$ and $\kappa_2 = \cos^2 \theta / C^2 + \sin^2 \theta / B^2$. Substituting back,

$$\begin{aligned}
\int_S r^2 d\omega &= 4\pi \int_0^{\pi/2} \frac{\sin \theta d\theta}{(\sin^2 \theta/A^2 + \cos^2 \theta/C^2)^{1/2} (\cos^2 \theta/C^2 + \sin^2 \theta/B^2)^{1/2}} \\
&= 4\pi \int_0^{\pi/2} \frac{\sin \theta \sec^2 \theta d\theta}{(\tan^2 \theta/A^2 + 1/C^2)^{1/2} (1/C^2 + \tan^2 \theta/B^2)^{1/2}} \\
&= 4\pi ABC^2 \int_0^{\pi/2} \frac{\sin \theta \sec^2 \theta d\theta}{(C^2 \tan^2 \theta + A^2)^{1/2} (C^2 \tan^2 \theta + B^2)^{1/2}} \\
&= 4\pi ABC \int_0^{\pi/2} \frac{2C^2 \sin \theta \sec^3 \theta d\theta}{2C \sec \theta (C^2 \tan^2 \theta + A^2)^{1/2} (C^2 \tan^2 \theta + B^2)^{1/2}} \\
&= 2\pi ABC \int_0^{\pi/2} \frac{2C^2 \sin \theta \sec^3 \theta d\theta}{(C^2 \tan^2 \theta + C^2)^{1/2} (C^2 \tan^2 \theta + A^2)^{1/2} (C^2 \tan^2 \theta + B^2)^{1/2}}
\end{aligned}$$

Now substituting

$$u = C^2 \tan^2 \theta,$$

$$du = 2C^2 \sin \theta \sec^3 \theta d\theta \text{ and}$$

$$\begin{aligned}
\Delta &= (C^2 \tan^2 \theta + C^2)^{1/2} (C^2 \tan^2 \theta + A^2)^{1/2} (C^2 \tan^2 \theta + B^2)^{1/2} \\
&= (u + C^2)^{1/2} (u + A^2)^{1/2} (u + B^2)^{1/2}
\end{aligned}$$

$$\begin{aligned}
\int_S r^2 d\omega &= 2\pi ABC \int_0^\infty \frac{du}{\Delta} \\
&= 2\pi \chi_0
\end{aligned} \tag{5.4}$$

$$\text{where } \chi_0 = ABC \int_0^\infty \frac{du}{\Delta}.$$

Putting this in equation (2),

$$\Phi_{int} = -\pi G \rho (1 - m^2) \chi_0 \tag{5.5}$$

Now, we introduce a set of new constants α_0, β_0 and γ_0 , so that the integral can be expressed in terms of ratios of semi-axes of the ellipsoid. It can be shown that

$$\alpha_0 A^2 + \beta_0 B^2 + \gamma_0 C^2 = \chi_0 \quad (5.6)$$

where,

$$\begin{aligned} \alpha_0 &= \frac{I}{A^2} - \frac{1}{A} \frac{\delta \chi_0}{\delta A} \\ \beta_0 &= \frac{I}{B^2} - \frac{1}{B} \frac{\delta \chi_0}{\delta B} \\ \gamma_0 &= \frac{I}{C^2} - \frac{1}{C} \frac{\delta \chi_0}{\delta C} \end{aligned} \quad (5.7)$$

References

- Bruce Balick and Adam Frank. Shapes and shaping of planetary nebulae. *Annual Review of Astronomy and Astrophysics*, 40(1):439–486, September 2002. doi: 10.1146/annurev.astro.40.060401.093849. URL <https://doi.org/10.1146/annurev.astro.40.060401.093849>.
- Krzysztof Belczynski, Alessandra Buonanno, Matteo Cantiello, Chris L. Fryer, Daniel E. Holz, Ilya Mandel, M. Coleman Miller, and Marek Walczak. THE FORMATION AND GRAVITATIONAL-WAVE DETECTION OF MASSIVE STELLAR BLACK HOLE BINARIES. *The Astrophysical Journal*, 789(2):120, June 2014. doi: 10.1088/0004-637x/789/2/120. URL <https://doi.org/10.1088/0004-637x/789/2/120>.
- James Binney and Scott Tremaine. *Galactic dynamics*, volume 20. Princeton university press, 2011.
- Eric G. Blackman, Adam Frank, and Carl Welch. Magnetohydrodynamic stellar and disk winds: Application to planetary nebulae. *The Astrophysical Journal*, 546(1):288–298, January 2001. doi: 10.1086/318253. URL <https://doi.org/10.1086/318253>.
- Nadia Blagorodnova, R Kotak, J Polshaw, Mansi M Kasliwal, Y Cao, Ann Marie Cody, GB Doran, N Elias-Rosa, M Fraser, Christoffer Fremling, et al. Common envelope ejection for a luminous red nova in m101. *The Astrophysical Journal*, 834(2):107, 2017a.
- Nadia Blagorodnova, R Kotak, J Polshaw, Mansi M Kasliwal, Y Cao, Ann Marie Cody, GB Doran, N Elias-Rosa, M Fraser, Christoffer Fremling, et al. Common

- envelope ejection for a luminous red nova in m101. *The Astrophysical Journal*, 834(2):107, 2017b.
- Bohdan Paczynski. Structure and evolution of close binary systems. reidel, dordrecht. page 75, 1976.
- H. Bondi. On spherically symmetrical accretion. *Monthly Notices of the Royal Astronomical Society*, 112(2):195–204, April 1952. doi: 10.1093/mnras/112.2.195. URL <https://doi.org/10.1093/mnras/112.2.195>.
- H. Bondi and F. Hoyle. On the mechanism of accretion by stars. *Monthly Notices of the Royal Astronomical Society*, 104(5):273–282, October 1944. doi: 10.1093/mnras/104.5.273. URL <https://doi.org/10.1093/mnras/104.5.273>.
- GE Brown. Neutron star accretion and binary pulsar formation. *The Astrophysical Journal*, pages 270–279, February 1995.
- Jonathan J. Carroll-Nellenback, Brandon Shroyer, Adam Frank, and Chen Ding. Efficient parallelization for AMR MHD multiphysics calculations implementation in AstroBEAR. *Journal of Computational Physics*, 236:461–476, March 2013. doi: 10.1016/j.jcp.2012.10.004. URL <https://doi.org/10.1016/j.jcp.2012.10.004>.
- Luke Chamandy, Adam Frank, Eric G Blackman, Jonathan Carroll-Nellenback, Baowei Liu, Yisheng Tu, Jason Nordhaus, Zhuo Chen, and Bo Peng. Accretion in common envelope evolution. *Monthly Notices of the Royal Astronomical Society*, 480(2):1898–1911, July 2018. doi: 10.1093/mnras/sty1950. URL <https://doi.org/10.1093/mnras/sty1950>.
- Luke Chamandy, Eric G Blackman, Adam Frank, Jonathan Carroll-Nellenback, Yanguxin Zou, and Yisheng Tu. How drag force evolves in global common en-

velope simulations. *Monthly Notices of the Royal Astronomical Society*, 490(3):3727–3739, October 2019a. doi: 10.1093/mnras/stz2813. URL <https://doi.org/10.1093/mnras/stz2813>.

Luke Chamandy, Yisheng Tu, Eric G Blackman, Jonathan Carroll-Nellenback, Adam Frank, Baowei Liu, and Jason Nordhaus. Energy budget and core-envelope motion in common envelope evolution. *Monthly Notices of the Royal Astronomical Society*, 486(1):1070–1085, March 2019b. doi: 10.1093/mnras/stz887. URL <https://doi.org/10.1093/mnras/stz887>.

Luke Chamandy, Eric G Blackman, Adam Frank, Jonathan Carroll-Nellenback, and Yisheng Tu. Common envelope evolution on the asymptotic giant branch: unbinding within a decade? *Monthly Notices of the Royal Astronomical Society*, 495(4):4028–4039, May 2020. doi: 10.1093/mnras/staa1273. URL <https://doi.org/10.1093/mnras/staa1273>.

S. Chandrasekhar. Dynamical friction. i. general considerations: the coefficient of dynamical friction. *The Astrophysical Journal*, 97:255, March 1943. doi: 10.1086/144517. URL <https://doi.org/10.1086/144517>.

S. Chandrasekhar. *Ellipsoidal Figures of Equilibrium*. Yale University Press, New Haven, first edition, 1969. ISBN 978-0300012281.

Andrew J. Cunningham, Adam Frank, Peggy Varnière, Sorin Mitran, and Thomas W. Jones. SIMULATING MAGNETOHYDRODYNAMICAL FLOW WITH CONSTRAINED TRANSPORT AND ADAPTIVE MESH REFINEMENT: ALGORITHMS AND TESTS OF THE AstroBEAR CODE. *The Astrophysical Journal Supplement Series*, 182(2):519–542, May 2009. doi: 10.1088/0067-0049/182/2/519. URL <https://doi.org/10.1088/0067-0049/182/2/519>.

- M De Kool. Common envelope evolution and double cores of planetary nebulae. *The Astrophysical Journal*, 358:189–195, 1990.
- J. D. M. Dewi, P. Podsiadlowski, and A. Sena. Double-core evolution and the formation of neutron star binaries with compact companions. *Monthly Notices of the Royal Astronomical Society*, 368(4):1742–1748, June 2006. doi: 10.1111/j.1365-2966.2006.10233.x. URL <https://doi.org/10.1111/j.1365-2966.2006.10233.x>.
- Richard Edgar. A review of bondi–hoyle–lyttleton accretion. *New Astronomy Reviews*, 48(10):843–859, September 2004. doi: 10.1016/j.newar.2004.06.001. URL <https://doi.org/10.1016/j.newar.2004.06.001>.
- Andrés Escala, Richard B Larson, Paolo S Coppi, and Diego Mardones. The role of gas in the merging of massive black holes in galactic nuclei. i. black hole merging in a spherical gas cloud. *The Astrophysical Journal*, 607(2):765, 2004.
- Kelly M Hambleton, Federica B Bianco, Rachel Street, Keaton Bell, David Buckley, Melissa Graham, Nina Hernitschek, Michael B Lund, Elena Mason, Joshua Pepper, et al. Rubin observatory lsst transients and variable stars roadmap. *arXiv preprint arXiv:2208.04499*, 2022.
- Z. Han and Ph. Podsiadlowski. The single-degenerate channel for the progenitors of type ia supernovae. *Monthly Notices of the Royal Astronomical Society*, 350(4):1301–1309, June 2004. doi: 10.1111/j.1365-2966.2004.07713.x. URL <https://doi.org/10.1111/j.1365-2966.2004.07713.x>.
- F. Hoyle and R. A. Lyttleton. The effect of interstellar matter on climatic variation. *Mathematical Proceedings of the Cambridge Philosophical Society*, 35(3):405–415,

- July 1939. doi: 10.1017/s0305004100021150. URL <https://doi.org/10.1017/s0305004100021150>.
- F. Hoyle and R. A. Lyttleton. On the physical aspects of accretion by stars. *Mathematical Proceedings of the Cambridge Philosophical Society*, 36(4):424–437, October 1940. doi: 10.1017/s0305004100017461. URL <https://doi.org/10.1017/s0305004100017461>.
- Roberto Iaconi, Thomas Reichardt, Jan Staff, Orsola De Marco, Jean-Claude Passy, Daniel Price, James Wurster, and Falk Herwig. The effect of a wider initial separation on common envelope binary interaction simulations. *Monthly Notices of the Royal Astronomical Society*, 464(4):4028–4044, September 2016. doi: 10.1093/mnras/stw2377. URL <https://doi.org/10.1093/mnras/stw2377>.
- Roberto Iaconi, Orsola De Marco, Jean-Claude Passy, and Jan Staff. The effect of binding energy and resolution in simulations of the common envelope binary interaction. *Monthly Notices of the Royal Astronomical Society*, 477(2):2349–2365, March 2018. doi: 10.1093/mnras/sty794. URL <https://doi.org/10.1093/mnras/sty794>.
- I. Iben and M. Livio. Common envelope evolution: where we stand and how we can move forward. *The Astronomy and Astrophysics Review*, pages 1373–1406, December 1993.
- I. Iben and AV Tutukov. Supernovae of type i as end products of the evolution of binaries with components of moderate initial mass ($m \gtrsim m_0$). *The Astrophysical Journal Supplement Series*, pages 335–372, September 1984.
- N. Ivanova. COMMON ENVELOPE: ON THE MASS AND THE FATE OF THE

- REMNANT. *The Astrophysical Journal*, 730(2):76, March 2011. doi: 10.1088/0004-637x/730/2/76. URL <https://doi.org/10.1088/0004-637x/730/2/76>.
- N. Ivanova, S. Justham, X. Chen, O. De Marco, C. L. Fryer, E. Gaburov, H. Ge, E. Glebbeek, Z. Han, X.-D. Li, G. Lu, T. Marsh, P. Podsiadlowski, A. Potter, N. Soker, R. Taam, T. M. Tauris, E. P. J. van den Heuvel, and R. F. Webbink. Common envelope evolution: where we stand and how we can move forward. *The Astronomy and Astrophysics Review*, 21(1), February 2013. doi: 10.1007/s00159-013-0059-2. URL <https://doi.org/10.1007/s00159-013-0059-2>.
- Natalia Ivanova, Stephen Justham, and Paul Ricker. *Common Envelope Evolution*. IOP Publishing, 2020.
- David Jones and Henri M. J. Boffin. Binary stars as the key to understanding planetary nebulae. *Nature Astronomy*, 1(5), May 2017. doi: 10.1038/s41550-017-0117. URL <https://doi.org/10.1038/s41550-017-0117>.
- V Kalogera, K Belczynski, C Kim, R Oshaughnessy, and B Willems. Formation of double compact objects. *Physics Reports*, 442(1-6):75–108, April 2007. doi: 10.1016/j.physrep.2007.02.008. URL <https://doi.org/10.1016/j.physrep.2007.02.008>.
- Amit Kashi and Noam Soker. Operation of the jet feedback mechanism (jfm) in intermediate luminosity optical transients (ilots). *Research in Astronomy and Astrophysics*, 16(6):014, 2016.
- Mansi Kasliwal. Spitzer infrared intensive transients survey. *Keck Observatory Archive DEIMOS C346D*, page 395, 2016.

Mansi M Kasliwal, John Bally, Frank Masci, Ann Marie Cody, Howard E Bond, Jacob E Jencson, Samaporn Tinyanont, Yi Cao, Carlos Contreras, Devin A Dykhoff, et al. Spirits: Uncovering unusual infrared transients with spitzer. *The Astrophysical Journal*, 839(2):88, 2017.

Gustav Kirchhoff. Über das gleichgewicht und die bewegung einer elastischen scheibe. *Journal für die reine und angewandte Mathematik*, 119:51–88, 1897.

Horace Lamb. *Hydrodynamics*. Cambridge University Press, Cambridge, UK, 1879.

Mario Livio and Noam Soker. The common envelope phase in the evolution of binary stars. *The Astrophysical Journal*, 329:764–779, 1988.

JC Lombardi Jr, ZF Proulx, KL Dooley, EM Theriault, N Ivanova, and FA Rasio. Stellar collisions and ultracompact x-ray binary formation. *The Astrophysical Journal*, 640(1):441, 2006.

Morgan MacLeod and Enrico Ramirez-Ruiz. ON THE ACCRETION-FED GROWTH OF NEUTRON STARS DURING COMMON ENVELOPE. *The Astrophysical Journal*, 798(1):L19, December 2014. doi: 10.1088/2041-8205/798/1/l19. URL <https://doi.org/10.1088/2041-8205/798/1/l19>.

Morgan MacLeod and Enrico Ramirez-Ruiz. ASYMMETRIC ACCRETION FLOWS WITHIN a COMMON ENVELOPE. *The Astrophysical Journal*, 803(1):41, April 2015. doi: 10.1088/0004-637x/803/1/41. URL <https://doi.org/10.1088/0004-637x/803/1/41>.

Morgan MacLeod, Andrea Antoni, Ariadna Murguia-Berthier, Phillip Macias, and Enrico Ramirez-Ruiz. Common envelope wind tunnel: Coefficients of drag and accretion in a simplified context for studying flows around objects embedded within

- stellar envelopes. *The Astrophysical Journal*, 838(1):56, March 2017. doi: 10.3847/1538-4357/aa6117. URL <https://doi.org/10.3847/1538-4357/aa6117>.
- X. Meng and Ph. Podsiadlowski. A common-envelope wind model for type ia supernovae – i. binary evolution and birth rate. *Monthly Notices of the Royal Astronomical Society*, 469(4):4763–4787, May 2017. doi: 10.1093/mnras/stx1137. URL <https://doi.org/10.1093/mnras/stx1137>.
- J. Nordhaus and E. G. Blackman. Low-mass binary-induced outflows from asymptotic giant branch stars. *Monthly Notices of the Royal Astronomical Society*, 370(4):2004–2012, July 2006. doi: 10.1111/j.1365-2966.2006.10625.x. URL <https://doi.org/10.1111/j.1365-2966.2006.10625.x>.
- J. Nordhaus, E. G. Blackman, and A. Frank. Isolated versus common envelope dynamos in planetary nebula progenitors. *Monthly Notices of the Royal Astronomical Society*, 376(2):599–608, April 2007. doi: 10.1111/j.1365-2966.2007.11417.x. URL <https://doi.org/10.1111/j.1365-2966.2007.11417.x>.
- Sebastian T Ohlmann, Friedrich K Röpke, Rüdiger Pakmor, and Volker Springel. Constructing stable 3d hydrodynamical models of giant stars. *Astronomy & Astrophysics*, 599:A5, 2017.
- Eve C Ostriker. Dynamical friction in a gaseous medium. *The Astrophysical Journal*, 513(1):252, 1999.
- Andrea Pastorello, T-W Chen, Y-Z Cai, A Morales-Garoffolo, Z Cano, Elena Mason, EA Barsukova, Stefano Benetti, M Berton, S Bose, et al. The evolution of luminous red nova at 2017jfs in ngc 4470. *Astronomy & Astrophysics*, 625:L8, 2019.

- Frederic A Rasio and Mario Livio. On the formation and evolution of common envelope systems. *The Astrophysical Journal*, 471(1):366, 1996.
- Thomas A Reichardt, Orsola De Marco, Roberto Iaconi, Christopher A Tout, and Daniel J Price. Extending common envelope simulations from roche lobe overflow to the nebular phase. *Monthly Notices of the Royal Astronomical Society*, 484(1):631–647, December 2018. doi: 10.1093/mnras/sty3485. URL <https://doi.org/10.1093/mnras/sty3485>.
- M. Reyes-Ruiz and J. A. López. Accretion disks in pre–planetary nebulae. *The Astrophysical Journal*, pages 952–960, December 1999.
- Paul M. Ricker and Ronald E. Taam. The interaction of stellar objects within a common envelope. *The Astrophysical Journal*, 672(1):L41–L44, December 2007. doi: 10.1086/526343. URL <https://doi.org/10.1086/526343>.
- Paul M. Ricker and Ronald E. Taam. AN AMR STUDY OF THE COMMON-ENVELOPE PHASE OF BINARY EVOLUTION. *The Astrophysical Journal*, 746(1):74, January 2012. doi: 10.1088/0004-637x/746/1/74. URL <https://doi.org/10.1088/0004-637x/746/1/74>.
- A. J. Ruiter, K. Belczynski, S. A. Sim, W. Hillebrandt, C. L. Fryer, M. Fink, and M. Kromer. Delay times and rates for type ia supernovae and thermonuclear explosions from double-detonation sub-chandrasekhar mass models. *Monthly Notices of the Royal Astronomical Society*, 417(1):408–419, August 2011. doi: 10.1111/j.1365-2966.2011.19276.x. URL <https://doi.org/10.1111/j.1365-2966.2011.19276.x>.
- Eric L Sandquist, Ronald E Taam, Xingming Chen, Peter Bodenheimer, and An-

- Andreas Burkert. Double core evolution. x. through the envelope ejection phase. *The Astrophysical Journal*, 500(2):909, 1998.
- Eric L Sandquist, Ronald E Taam, and Andreas Burkert. On the formation of helium double degenerate stars and pre-cataclysmic variables. *The Astrophysical Journal*, 533(2):984, 2000.
- HE Schwarz, RLM Corradi, and J Melnick. A catalogue of narrow band images of planetary nebulae. *Astronomy and Astrophysics Supplement Series*, 96:23–113, 1992.
- N. Soker. Influences of wide binaries on the structures of planetary nebulae. *Monthly Notices of the Royal Astronomical Society*, 270(4):774–780, October 1994. doi: 10.1093/mnras/270.4.774. URL <https://doi.org/10.1093/mnras/270.4.774>.
- N. Soker and S. Rappaport. The formation of very narrow waist bipolar planetary nebulae. *The Astrophysical Journal*, pages 241–259, February 2000.
- N. Soker and S. Rappaport. Departure from axisymmetry in planetary nebulae. *The Astrophysical Journal*, pages 256–265, April 2001.
- Noam Soker and Amit Kashi. Explaining two recent intermediate-luminosity optical transients (ilots) by a binary interaction and jets. *Monthly Notices of the Royal Astronomical Society*, 462(1):217–222, 2016.
- Volker Springel. Smoothed particle hydrodynamics in astrophysics. *Annual Review of Astronomy and Astrophysics*, 48:391–430, 2010.
- Ronald F Webbink. Evolution of helium white dwarfs in close binaries. *Monthly Notices of the Royal Astronomical Society*, 171(3):555–568, 1975.

REFERENCES

Adolf N. Witt, Uma P. Vijh, L. M. Hobbs, Jason P. Aufdenberg, Julie A. Thorburn, and Donald G. York. THE RED RECTANGLE: ITS SHAPING MECHANISM AND ITS SOURCE OF ULTRAVIOLET PHOTONS. *The Astrophysical Journal*, 693(2):1946–1958, March 2009. doi: 10.1088/0004-637x/693/2/1946. URL <https://doi.org/10.1088/0004-637x/693/2/1946>.